
PERGAMON

Journal of Quantitative Spectroscopy & Radiative Transfer 65 (2000) 693–728

Journal of Quantitative Spectroscopy & Radiative Transfer

www.elsevier.com/locate/jqsrt

Adjoint perturbation and selection rule methods for solar broadband two-stream fluxes in multi-layer media

Philip Gabriel*, Graeme L. Stephens, Ian L. Wittmeyer

Department of Atmospheric Science, Colorado State University, Fort Collins, CO 80523, USA

Abstract

This paper describes computationally efficient methods of solving the two-stream plane-parallel equation of radiative transfer in multi-layered media using adjoint perturbations in combination with selection rules. Semi-analytical results are obtained for the perturbed fluxes in atmospheres illuminated by solar radiation. The perturbation approach is useful in media dominated by multiple scattering whereas selection rules apply when absorption is dominant or if the media is weakly scattering. Selection rules can be applied with conventional two-stream solvers to reduce the number of radiative transfer calculations. For example, clear sky broadband fluxes computed with selection rules for a 30 layer atmosphere using the *k*-distribution method were obtained in about one-seventh the time taken by the standard solvers. An 12-fold increase in computational speed over the standard solvers was achieved when selection rules were used with the perturbation method for the same atmosphere. Fluxes so computed were within 10% of those calculated using standard, full up two-stream radiative transfer codes.

1. Introduction

The need for simple, robust and computationally efficient methods for solving a variety of radiative transfer problems has been underscored by Gabriel et al. [1]. The method of adjoint perturbations used here to obtain approximate solutions to the two-stream fluxes was introduced to the atmospheric science community by Box et al. [2], and Gerstel [3], although its theoretical development arose from neutron transport studies [4]. The technique has been applied to the computation of monochromatic fluxes in optically thin atmospheres (e.g. [5]). Perturbations were defined by changing the composition of the atmosphere through changes in the ozone or aerosol profiles from given base-state profiles. Those studies showed the approach to be surprisingly

* Corresponding author. Tel.: + 1-970-491-3392; fax: + 1-970-491-8449.

0022-4073/00/$ - see front matter
PII: S0022-4073(99)00137-5

accurate over a large range of perturbations. More recently, Box et al. [6] calculated spectrally integrated ultra violet fluxes at the surface and introduced perturbations as a way of dealing with spectrally varying ozone absorption. The objective of the present work is to understand and use the properties of the adjoint perturbation to calculate broadband fluxes in multi-layer atmospheres. It is an extension of the work of Gabriel et al. [1] who applied the method successfully in obtaining broadband fluxes in a single-layer medium.

The adjoint perturbation model is presented in three sections: Section 2 introduces terminology and focuses on obtaining a continuous solution for the fluxes in a form required to derive the adjoint perturbations, Section 3 formulates and solves the adjoint equation, and Section 4 develops the perturbation approximation from the definition of both physical and adjoint fluxes. Section 5 introduces a new semi-empirical algorithm called the selection rules method applicable to those problems dominated by absorption. Selection rules eliminate the need for performing detailed radiative transfer computations and can be used with either standard methods for computing the fluxes or in conjunction with the adjoint perturbation method. Section 6 compares flux profiles obtained by the adding algorithm to those obtained by the combined perturbation and selection rules methods. A summary and conclusion is provided in Section 7.

2. Base state

The goal of the perturbation method is to calculate fluxes efficiently by performing radiative transfer calculations only once on what is termed the base state. The fluxes associated with a different optical profile (the final state) are then determined by perturbing those of the base state with a transition operator that contains information about the desired, final state. The base state Ξ is defined collectively by an initial flux profile F_0, the initial distribution of optical properties X_i, and boundary conditions $F^{\pm}_{\mathrm{bc}}$. Functions that are dependent the initial distribution of optical properties are also considered as a part of the base state. For example, the adjoint operator $\mathscr{F}_0$ and the Greens function G_0 are associated with the base state, and it is understood that flux profiles of

Fig. 1. (a) Conceptual overview of the adjoint perturbation method. The base state is denoted by Ξ_i. Optical properties of the base state are denoted by χ_i. The arguments of χ_i depend on the scattering, and extinction coefficients as well as the asymmetry factor of the layers. Function χ is used in the definition of a specific two-stream model. Associated with the base state are the boundary conditions, F_{bc}, the flux distribution, F_0, the adjoint flux, $\mathscr{F}_0$, and other functions of the optical properties required by the perturbation, denoted by $\mathscr{O}_i$. The transition operator that takes Ξ_i into the final state Ξ_f is $\Delta L[\chi_f - \chi_i]$, a simple matrix of the difference between the final and base state optical properties. The fluxes of the final state, $F_0 + \Delta F$, are calculated by the inner product shown in the arrow. The lower figure illustrates the sequence of steps required to calculate the perturbed fluxes. In the first box are specified the base-state optical properties and the boundary conditions. In the second box, the base-state fluxes and adjoint fluxes are calculated. The transition operator is then used to compute the inner product from which follows the perturbed flux. The inner product is computed as shown in the upper figure. (b) Illustration of the labelling convention used in the development of the adjoint perturbation method. The values of z increase from the base to the top of the atmosphere. The arrows shown in layer two emphasize that the upwelling and downwelling fluxes and adjoint fluxes associated with layers 1 and 2 must match at the interface located at $z = z_2$. Such matchings, in fact, occurs at all internal boundaries and are the key to obtaining the semi-analytical solutions for the fluxes and adjoint fluxes described in the text.

the final state will respect the boundary conditions of the base state. Box et al. [7] shows how the base state is used to compute a final flux profile in terms of differences in the distribution of optical properties. This concept is illustrated in Fig. 1a. The transition operator denoted by ΔL in the figure is a matrix whose detailed structure is given later in this paper.

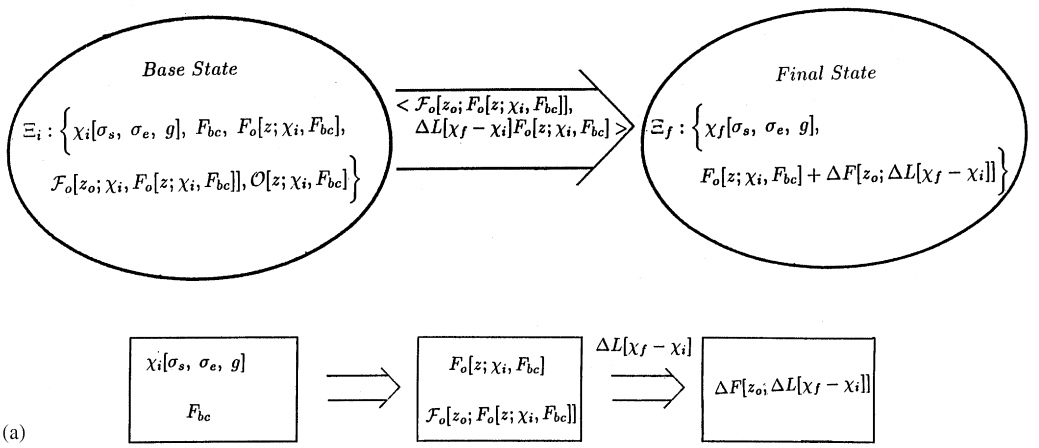

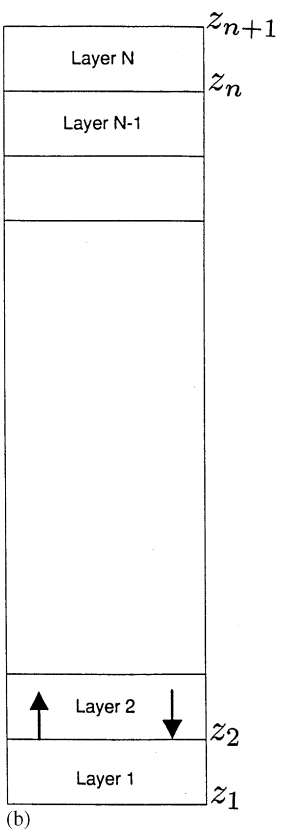

The infinite series from which the perturbation approximation derives was obtained by Box et al. [7]. The series is

$$F = F_0 - \langle \mathscr{F}_0, \Delta L F_0 \rangle + \langle \mathscr{F}_0, \Delta L G_0 \Delta L F_0 \rangle - \langle \mathscr{F}_0, \Delta L G_0 \Delta L G_0 \Delta L F_0 \rangle + \cdots . \tag{1}$$

The brackets containing vector arguments X and Y, $\langle X, Y \rangle$ indicate the taking of their inner, or dot product. If all the terms in the series are considered, Eq. (1) yields the *exact* solution for the final-state fluxes. In what follows, only the first two terms of the series will be retained. The omission of higher-order terms constitutes the perturbation approximation. Higher-order terms require the calculation of the Greens function, and although this function can be derived, the inclusion of such terms will compromise computational efficiency. However, as will be discussed in Section 3, there is a semi-empirical correction that can improve the accuracy, but at the expense of introducing additional computations of exponential terms.

2.1. Continuous flux solution

This section develops a continuous analytic solution for the fluxes in an inhomogeneous multilayer atmosphere. The solution to this problem is, of course, well known and is usually given in dimensionless optical depth coordinates. However, in the calculation of the perturbations, the solution must be expressed in physical coordinates. Since the analytical form of the solution to the perturbation method depends on that of the two-stream fluxes, derivation of the latter is necessary for understanding and reproducing the formulae to be presented. Finally, the solution of the adjoint parallels that of the solution of the physical flux, and this helps to reduce the length of that section. Calculation of the two-stream fluxes (herein limited to the solar problem but extended in a later paper to infrared transfer), begins with the canonical form of the differential equation that defines them. Beginning with a single layer, with its upper boundary at z_t and its lower boundary at $z = z_1$, we have

$$LF_0 = Q_0, \tag{2}$$

where F_0 is the vector

$$F_0 = \begin{pmatrix} F^+(z) \\ F^-(z) \end{pmatrix}$$

of upwelling $F^+(z)$ and downwelling $F^-(z)$ fluxes at level z. The solar source vector is given by

$$Q_0 = \begin{pmatrix} \gamma_3 \\ -\gamma_4 \end{pmatrix} f_0 \exp[\kappa(z - z_t)], \tag{3a}$$

where $\kappa = \sigma_e/\mu_0$, $\gamma_3 = 0.25(2 - 3g\mu_0)$ and $\gamma_4 = 0.25(2 + 3g\mu_0)$, while the two-stream operator is

$$L = I\frac{\mathrm{d}}{\mathrm{d}z} - A. \tag{3b}$$

Here I is the identity matrix and matrix A is a 2×2 attenuation operator defined by

$$A = \begin{pmatrix} -\gamma_1 & \gamma_2 \\ -\gamma_2 & \gamma_1 \end{pmatrix} \tag{3c}$$

with $\gamma_1 = 0.25(7\sigma_e - \sigma_s(4 + 3g))$ and $\gamma_2 = -0.25(\sigma_e - \sigma_s(4 - 3g))$.

The solution for a single homogeneous layer can be determined by pre-multiplying Eq. (2) by the integrating factor $\exp[-Az]$ and using the expansion:

$$\frac{\mathrm{d}}{\mathrm{d}z}(\exp[-Az]F_0) = \exp[-Az]\left(\frac{\mathrm{d}F_0}{\mathrm{d}z} - AF_0\right) \tag{4}$$

which yields

$$\frac{\mathrm{d}}{\mathrm{d}z}(\exp[-Az]F_0) = \exp[-Az]Q_0. \tag{5}$$

Integrating this expression results in the flux:

$$F_0 = \exp[Az]C + (\kappa I - A)^{-1}Q_0. \tag{6}$$

The components of vector C in Eq. (6) may be determined from the boundary conditions that the diffuse flux must satisfy at the base and top of the medium. The exponential matrix can be evaluated by using the Cayley–Hamilton Theorem. It may also be calculated by using fundamental roperties of the two-stream A matrix, namely

$$A^m = \lambda^m I, \quad m = 0, 2, 4, \ldots, \tag{7a}$$

$$A^n = \lambda^n I, \quad n = 1, 3, 5, \ldots, \tag{7b}$$

$$AB + BA = 2(\gamma_1\eta_1 - \gamma_2\eta_2)I, \tag{7c}$$

where matrix B is isomorphic to A, having elements

$$B = \begin{pmatrix} -\eta_1 & \eta_2 \\ -\eta_2 & \eta_1 \end{pmatrix}.$$

Expression (7a) and (7b) are used in the computation of the matrix exponential and inverse matrix in (6) when those terms are expanded in a Taylor series about the origin. The results are:

$$\exp[Az] = \cosh(\lambda z)I + \frac{\sinh(\lambda z)}{\lambda}A \tag{7d}$$

and

$$(\kappa I - A)^{-1} = \begin{pmatrix} \beta_{1,1} & \beta_{1,2} \\ \beta_{2,1} & \beta_{2,2} \end{pmatrix}, \tag{7e}$$

where

$$\beta_{1,1} = \frac{\gamma_1 - \kappa}{\Delta}, \qquad \beta_{1,2} = \frac{-\gamma_2}{\Delta},$$

$$\beta_{2,1} = \frac{\gamma_2}{\Delta}, \qquad \beta_{2,2} = \frac{\gamma_1 - \kappa}{\Delta} \tag{7f}$$

with the eigenvalue $\lambda^2 = \gamma_1^2 - \gamma_2^2$ and $\Delta = \lambda^2 - \kappa^2$. Although expression (7c) is not used, it is reported here because it enters in the solution of the more general problem of solving the fluxes when the A matrix is not constant as above, but rather is dependent on z explicitly. The analytical solution made possible by this relation is the subject of another study. The two-stream solution for a single layer is

$$\begin{pmatrix} F^+(z) \\ F^-(z) \end{pmatrix} = \begin{pmatrix} e_{1,1}(z) & e_{1,2}(z) \\ e_{2,1}(z) & e_{2,2}(z) \end{pmatrix} \begin{pmatrix} C^+ \\ C^- \end{pmatrix} + \begin{pmatrix} \beta_{1,1} & \beta_{1,2} \\ \beta_{2,1} & \beta_{2,2} \end{pmatrix} Q_0, \tag{8a}$$

where the components of the exponential matrix are given by

$$e_{1,1}(z) = p_1 \exp(\lambda z) + p_2 \exp(-\lambda z),$$

$$e_{1,2}(z) = p_3(\exp(\lambda z) - \exp(-\lambda z)),$$

$$e_{2,1}(z) = p_3(\exp(-\lambda z) - \exp(\lambda z)),$$

$$e_{2,2}(z) = p_2 \exp(\lambda z) + p_1 \exp(-\lambda z).$$

The constants in the above expressions are

$$p_1 = \frac{(\lambda - \gamma_1)}{2\lambda}, \qquad p_2 = \frac{(\lambda + \gamma_1)}{2\lambda}, \qquad p_3 = \frac{\gamma_2}{2\lambda}$$

and satisfy

$$p_1 p_2 + p_3^2 = 0, \qquad p_1^2 + p_2^2 - 2p_3^2 = 1.$$

The boundary conditions:

$$F^+(z_1) = R_g(F^-(z_t) + \exp(\kappa(z_t - z_1))), \tag{8b}$$

$$F^-(z_t) = F_{\text{down}} \tag{8c}$$

determine the coefficient vector C. Diffuse radiation entering the upper boundary is denoted by F_{down}, and the reflection of the lower boundary (assumed Lambertian) is denoted by R_g. Although the solution is mathematically complete, its numerical properties are unacceptable because of the presence of the growing exponential terms in the upwelling and downwelling fluxes. For a direct beam of unit strength, the fluxes must lie between zero and unity. This constraint will be violated when the optical thickness becomes large. A stable solution can be obtained, however, by reformulating the solutions in terms of reflection and transmission functions. This will be a straightforward task using the development already presented and will now be described for multiple layers.

Fig. 1b defines the multi-layered plane-parallel atmosphere used throughout this work. Level quantities are specified by z_i. The optical properties are taken to be constant within all layers, but may differ from layer to layer. Fluxes are specified using two indicies. For example, $F_1^+(z_2)$ designates the upwelling hemispherical flux associated with layer one at altitude z_2. Optical properties, and functions of these properties (e.g. λ_i, κ_i, etc.) are labelled by a single index, i that denotes the ith layer. Such an arrangement is necessary since the flux must be determined at any z, not just on boundaries. This goal is attainable if the equation of transfer is solved in every layer, keeping in mind that the source term at position z is determined by the vertical distribution of the extinction above z. To fix these ideas, the differential equations that define the fluxes in the ith layer are:

$$\frac{\mathrm{d}F_i^+(z)}{\mathrm{d}z} = -\gamma_1^i F_i^+ + \gamma_2^i F_i^- + \gamma_3^i f_0 W_i(z), \tag{9a}$$

$$\frac{\mathrm{d}F_i^-(z)}{\mathrm{d}z} = -\gamma_2^i F_i^+ + \gamma_1^i F_i^- - \gamma_4^i f_0 W_i(z), \tag{9b}$$

$$W_i(z) = W_{i+1}(z)\exp(\kappa_i(z - z_{i+1})), \tag{9c}$$

where $W_N(z_{N+1}) = W_{N+1}(z_{N+1}) = 1$. The quantity $W_i(z)$ accounts for the depletion of the direct beam (of magnitude given by f_0 at the top of the atmosphere) by the previous layers and is calculated by iteration with $W_{N+1}(z_{n+1}) = 1$. The solution for the fluxes in the ith layer may now be written analogously to (8a):

$$\begin{aligned} F_i^+(z) &= C_i^+ e_{1,1}^i(z) + C_i^- e_{1,2}^i(z) + (\beta_{1,1}^i \gamma_3^i - \beta_{1,2}^i \gamma_4^i) W_{i+1}(z_{i+1})\exp(\kappa_i(z - z_{i+1})) \\ &= C_i^+ e_{1,1}^i(z) + C_i^- e_{1,2}^i(z) - S_i^+(z), \end{aligned} \tag{10a}$$

$$\begin{aligned} F_i^-(z) &= C_i^+ e_{2,1}^i(z) + C_i^- e_{2,2}^i(z) + (\beta_{2,1}^i \gamma_3^i - \beta_{2,2}^i \gamma_4^i) W_{i+1}(z_{i+1})\exp(\kappa_i(z - z_{i+1})) \\ &= C_i^+ e_{2,1}^i(z) + C_i^- e_{2,2}^i(z) - S_i^-(z), \end{aligned} \tag{10b}$$

where the sources associated with the upwelling and downwelling fluxes are $S_i^+(z)$ and $S_i^-(z)$, respectively. The coefficients C_i^+ and C_i^- are arbitrary constants for the ith layer having dimensions of flux.

Two kinds of boundary conditions must be imposed to determine C_i^+ and C_i^-. The first requires that the fluxes be continuous accross the internal boundaries. The second specifies external boundary conditions. Continuity requires:

$$F_i^+(z_i) = F_{i-1}^+(z_i), \tag{11a}$$

$$F_i^-(z_i) = F_{i+1}^-(z_i), \tag{11b}$$

while the external boundary conditions are as given in (8b) with z_t replaced by z_{N+1}.

Applying the internal boundary conditions to Eqs. (10a) and (10b) and Cramer's rule, the coefficients C_i^+ and C_i^- are obtained. These coefficients are inserted back into (10a) and (10b), and with the aid of composition rules that relate the $e_{i,j}(z)$, the fluxes are obtained. One example of a composition rule is $e_{1,1}(x)e_{2,2}(y) - e_{2,1}(x)e_{1,2}(y) = e_{1,1}(x - y)$. Such relations are derived as

needed and are a part of the algebraic process that leads to the following form for the fluxes:

$$F_i^+(z) = T_1^i(z)F_{i-1}^+(z_i) + R_1^i(z)F_{i+1}^-(z_{i+1}) + S_i^+(z_i)T_1^i(z) + S_{i+1}^-(z_{i+1})R_1^i(z) - S_i^+(z), \tag{12a}$$

$$F_i^-(z) = R_2^i(z)F_{i-1}^+(z_i) + T_2^i(z)F_{i+1}^-(z_{i+1}) + S_i^+(z_i)R_2^i(z) + S_{i+1}^-(z_{i+1})T_2^i(z) - S_i^-(z) \tag{12b}$$

with

$$T_1^i(z) = \frac{p_1^i \exp(\lambda_i(z + z_i - 2z_{i+1})) + p_2^i \exp(\lambda_i(z_i - z))}{p_1^i \exp(2\lambda_i(z_i - z_{i+1})) + p_2^i}, \tag{13a}$$

$$R_1^i(z) = \frac{p_3^i(\exp(\lambda_i(z - z_{i+1})) - \exp(\lambda_i(2z_i - z - z_{i+1})))}{p_1^i \exp(2\lambda_i(z_i - z_{i+1})) + p_2^i}, \tag{13b}$$

$$T_2^i(z) = \frac{p_1^i \exp(\lambda_i(2z_i - z - z_{i+1})) + p_2^i \exp(\lambda_i(z - z_{i+1}))}{p_1^i \exp(2\lambda_i(z_i - z_{i+1})) + p_2^i}, \tag{13c}$$

$$R_2^i(z) = \frac{-p_3^i(\exp(\lambda_i(z_i + z - 2z_{i+1})) - \exp(\lambda_i(z_i - z)))}{p_1^i \exp(2\lambda_i(z_i - z_{i+1})) + p_2^i}. \tag{13d}$$

Eqs. (12) and (13) are statements of the interaction principle. Functions $R_1^i(z)$ and $R_2^i(z)$ are the global reflection functions of the ith layer, and $T_1^i(z)$, $T_2^i(z)$ are the global transmission functions. Since z must lie between z_i and z_{i+1}, the global reflection and transmission functions are bounded by zero and unity. The fluxes range bewteen zero and f_0, hence Eqs. (12a) and (12b) form a stable system that allow the boundary fluxes $F_i^+(z_i)$ and $F_i^-(z_i)$ to be calculated efficiently via a tri-diagonal solver. Note the use of $F_0^+(z_1) = F_1^+(z_1)$ (clearly there is no layer 0) when $i = 1$ as required by (11a). Then the flux at any position may be solved to within the accuracy afforded by the particular kind of two-stream model employed. The form of solution given by (12a) and (12b) is more efficient than the conventional adding method if evaluations of the flux are required at several arbitrary locations within a layer. In this case, the adding method would have to introduce additional layers so that the required positions lie on interfaces.

Selection of a two-stream model should be approached with some caution as it is possible to violate certain physical constraints. For example, the global reflection and transmission functions must be positive irrespective of position or the local optical properties. That this is not always the case is easily seen if attention is directed to the single layer with $z_1 = 0$ and $z_2 = z_t$. It is seen that

$$R_1(z) = \frac{p_3[\exp(\lambda(z - z_t)) - \exp(\lambda(-z - z_t))]}{p_1 \exp(-2\lambda z_t) + p_2}.$$

The quantity in square brackets in the numerator is always positive. The denominator is also positive, since $p_2 > p_1$ and p_1 is negative, as may be seen from the relations that the p_i satisfy. For the Delta–Eddington method, $R_1(z)$ will become negative when

$$\frac{1}{(4 - 3g)} - \frac{\sigma_s}{\sigma_e} > 0.$$

Quantities σ_e and σ_s denote the extinction and scattering coefficients of the layer. Similarly, $R_2(z)$ also becomes negative, while transmission functions retain positivity. If the aforementioned condition is true, upwelling and downwelling fluxes can be positive, but their accuracy may be

impaired. For example, when the asymmetry factor $g = 0$, the single-scattering albedo cannot be less than 0.25 without violating positivity requirements. These conditions can be encountered in clear sky radiative transfer. In multi-layer media, the effect of local violations of the aforementioned conditions on the accuracies of the computed fluxes is much more difficult to access. In these cases, even if the fluxes are everywhere positive, they may not be accurate at all positions due to long-range couplings of the global reflection and transmission functions. An example of this will be given in Section 4.

The preceeding discussion is relevant to the definition of the perturbations described below in as much as the accuracy of the perturbed fluxes depends on the base state fluxes. Not only are the internal fluxes required, but computation of the adjoint operators depend on accurate fluxes emerging from the boundaries of the medium. Finally, to complete this section, the form of solution for the diffuse fluxes used in the perturbation calculation is

$$F_i^+(z) = T_1^i(z)C_i^1 + R_1^i(z)C_i^2 + C_i^3\mathscr{X}_i(z), \tag{14a}$$

$$F_i^-(z) = R_2^i(z)C_i^1 + T_2^i(z)C_i^2 + C_i^4\mathscr{X}_i(z), \tag{14b}$$

where $\mathscr{X}_i(z) = \exp(\kappa_i(z - z_{i+1}))$. Eq. (14a) is the factored form of (12a).

Eq. (14b) is obtained from (12b) by adding to the latter the direct beam: $\mu_0 f_0 W_j \exp(\kappa_i(z - z_{i+1}))$. Coefficient C_i^4 is then identified as the factor multiplying the exponential. The downwelling direct radiation is added to the diffuse flux (i.e. (14b)) to yield the total flux.

2.2. Broadband solutions

Eqs. (14a) and (14b) can be used to calculate either spectral or broadband fluxes. The broadband flux vector $F_b(z)$ follows from the spectral fluxes using the k-distribution method (e.g. [8]) according to

$$F_b(z) = \int_{\lambda_{min}}^{\lambda_{max}} F_\lambda(z)\,d\lambda \sim \sum_{i=1}^{N_{bands}} \sum_{j=1}^{N_i} w_j F_j(z). \tag{14c}$$

Thus, broadband fluxes are obtained as a weighted sum over a discrete number of spectral intervals (or bands) and over a discrete number of radiative transfer computations for each interval. The relevant parameters are the number of bands denoted by N_{bands}, the number of absorption coefficients in each band that determine the optical properties and hence the number of radiative transfer calculations N_i, and the weights w_j whose sum is unity. The optical properties, although not explicitly stated in (14c), are implied in the calculation of $F_j(z)$. The results presented later employ the Fu and Liou k-distribution model [9]. For this model, a total of 54 independent flux calculations are required to compute the broadband solar fluxes and the properties of the model are summarized in Table 1.

3. Multi-layer adjoint solution

This section develops the adjoint solution of monochromatic transport on a multi-layer scattering and absorbing media as required in the perturbation approximation. The analytical properties

Table 1
Spectral division used in the calculation of broadband solar radiation. There are a total of 54 spectral lines

Band number	Wave number range (cm^{-1})	N_i
1	50 000–14 500	10
2	14 500–7700	8
3	7700–5250	12
4	5250–4000	7
5	4000–2850	12
6	2850–2500	5

of the adjoint fluxes are also explored to address issues concerning numerical stability. Use of the term "adjoint flux", hereafter designated by the symbol $\mathscr{F}_0$, is a misnomer since it is more appropriate to interpret $\mathscr{F}_0$ as an operator. However, in keeping with the the nomenclature established in Gabriel et al. [1], usage of this term will be retained. The adjoint operator formulation for a multi-layer medium can be derived by expanding the inner product,

$$\int_{z_1}^{z_{N+1}} (\mathscr{F}_0(z), LF_0(z))\,\mathrm{d}z,$$

as follows:

$$\int_{z_1}^{z_{N+1}} (\mathscr{F}_0(z), LF_0(z))\,\mathrm{d}z = \sum_{i=1}^{N} \int_{z_i}^{z_{i+1}} (\mathscr{F}_{0,i}(z), L_i F_{0,i}(z))\,\mathrm{d}z, \tag{15a}$$

where $\mathscr{F}_0$ is the 2×1 vector $(\mathscr{F}(z), \mathscr{F}(z))^{\mathrm{T}}$, L is a 2×2 matrix and LF_0 is equivalent to the source function by definition (2). The preceeding sum associates the adjoint fluxes, adjoint operator $L^{\dagger}$ and physical fluxes with the optical properties that characterize the ith layer. Next, each inner product is evaluated using integration by parts. For the ith layer, the result is

$$\int_{z_i}^{z_{i+1}} (\mathscr{F}_{0,i}(z), L_i F_{0,i}(z))\,\mathrm{d}z = \mathscr{F}_i^{+}(z)F_i^{+}(z)\big|_{z_i}^{z_{i+1}} + \mathscr{F}_i^{-}(z)F_i^{-}(z)\big|_{z_i}^{z_{i+1}} + \int_{z_i}^{z_{i+1}} (L_i^{\dagger}\mathscr{F}_{0,i}(z), F_{0,i}(z))\,\mathrm{d}z. \tag{15b}$$

The operator $L_i^{\dagger}$ is the adoint operator:

$$L_i^{\dagger} = -I\frac{\mathrm{d}}{\mathrm{d}z} - A_i^{\mathrm{T}}. \tag{16}$$

If Eq. (15b) is used repeatedly in (15a), all the internal bilinear concomitants cancel in pairs, with the exception of those at the upper and lower boundaries:

$$\int_{z_1}^{z_{N+1}} (\mathscr{F}_0(z), LF_0(z))\,\mathrm{d}z = (\mathscr{F}_N^+(z_{N+1})F_N^+(z_{N+1}) + \mathscr{F}_N^-(z_{N+1})F_N^-(z_{N+1})) - (\mathscr{F}_1^+(z_1)F_1^+(z_1) + \mathscr{F}_1^-(z_1)F_1^-(z_1)) + \sum_{i=1}^{N} \int_{z_i}^{z_{i+1}} (L_i^\dagger \mathscr{F}_{0,i}(z), F_{0,i}(z))\,\mathrm{d}z. \tag{17}$$

The inner product on the left side of the equality in (15a) can be used to calculate the physical fluxes through the identity $LF_0 = Q_0$, first setting the two bilinear concomitants in (15b) or (17) to zero and then letting

$$L_i^\dagger \mathscr{F}_0(z, z_0) = \delta(z - z_0)h, \tag{18}$$

where h is a vector having components $(h^+, h^-)^{\mathrm{T}}$. This vector determines whether the upwelling or downwelling flux is to be calculated. If the upwelling flux is desired then $h^+ = 1$ and $h^- = 0$. For the downwelling flux $h^+ = 0$ and $h^- = 1$. The delta function causes the sum in (15a) to vanish unless z_0, the position where the physical flux is to be calculated lies between levels z_i and z_{i+1}. The solution to (18) is

$$\mathscr{F}_i^+(z, z_0) = A_i^+ e_{2,2}^i(z) + A_i^- e_{1,2}^i(z) - (e_{2,2}^i(z - z_0)h^+ + e_{1,2}^i(z - z_0)h^-)H(z - z_0), \tag{19a}$$

$$\mathscr{F}_i^-(z, z_0) = A_i^+ e_{2,1}^i(z) + A_i^- e_{1,1}^i(z) - (e_{2,1}^i(z - z_0)h^+ + e_{1,1}^i(z - z_0)h^-)H(z - z_0). \tag{19b}$$

The solutions involve the Heaviside function. It is defined as

$$H(z) = \begin{cases} 1, & z \geq 0, \\ 0, & z < 0. \end{cases} \tag{20}$$

Coefficients A_i^+ and A_i^- are the arbitrary constants associated with the solution to the coupled first-order equations (18). They may be eliminated by asserting continuity in the adjoint fluxes:

$$\mathscr{F}_i^+(z_i, z_0) = \mathscr{F}_{i-1}^+(z_i, z_0), \tag{21a}$$

$$\mathscr{F}_i^-(z_i, z_0) = \mathscr{F}_{i-1}^-(z_i, z_0). \tag{21b}$$

Use of Cramer's rule to eliminate the coefficients leads to the interaction form of the solution, analogous to (12) for physical fluxes:

$$\mathscr{F}_i^+(z, z_0) = \mathscr{T}_i^1(z)\mathscr{F}_{i-1}^+(z_i, z_0) + \mathscr{R}_i^1(z)\mathscr{F}_{i+1}^-(z_{i+1}, z_0) + (e_{2,2}^i(z_i - z_0)h^+ + e_{1,2}^i(z_i - z_0)h^-)\mathscr{T}_i^1(z)H(z_i - z_0) - (e_{2,2}^i(z - z_0)h^+ + e_{1,2}^i(z - z_0)h^-)H(z - z_0) + (e_{2,1}^i(z_{i+1} - z_0)h^+ + e_{1,1}^i(z_{i+1} - z_0)h^-)\mathscr{R}_i^1(z)H(z_{i+1} - z_0), \tag{22a}$$

$$\begin{aligned}\mathscr{F}_i^-(z,z_0) = {} & \mathscr{R}_i^2(z)\mathscr{F}_{i-1}^+(z_i,z_0) + \mathscr{T}_i^1(z)\mathscr{F}_{i+1}^-(z_{i+1},z_0) \\ & + (e_{2,2}^i(z_i - z_0)h^+ + e_{1,2}^i(z_i - z_0)h^-)\mathscr{R}_i^2(z)H(z_i - z_0) \\ & - (e_{2,1}^i(z - z_0)h^+ + e_{1,1}^i(z - z_0)h^-)H(z - z_0) \\ & + (e_{2,1}^i(z_{i+1} - z_0)h^+ + e_{1,1}^i(z_{i+1} - z_0)h^-)\mathscr{T}_i^2(z)H(z_{i+1} - z_0), \end{aligned} \tag{22b}$$

where the adjoint global reflection $\mathscr{R}$ and transmission functions $\mathscr{T}$ are:

$$\mathscr{T}_1^i(z) = \frac{p_2^i \exp(\lambda_i(z + z_i - 2z_{i+1})) + p_1^i \exp(\lambda_i(z_i - z))}{p_2^i \exp(2\lambda_i(z_i - z_{i+1})) + p_1^i}, \tag{23a}$$

$$\mathscr{R}_1^i(z) = \frac{p_3^i(\exp(\lambda_i(z - z_{i+1})) - \exp(\lambda_i(2z_i - z - z_{i+1})))}{p_2^i \exp(2\lambda_i(z_i - z_{i+1})) + p_1^i}, \tag{23b}$$

$$\mathscr{T}_2^i(z) = \frac{p_2^i \exp(\lambda_i(2z_i - z - z_{i+1})) + p_1^i \exp(\lambda_i(z - z_{i+1}))}{p_2^i \exp(2\lambda_i(z_i - z_{i+1})) + p_1^i}, \tag{23c}$$

$$\mathscr{R}_2^i(z) = \frac{-p_3^i(\exp(\lambda_i(z_i + z - 2z_{i+1})) - \exp(\lambda_i(z_i - z)))}{p_2^i \exp(2\lambda_i(z_i - z_{i+1})) + p_1^i}. \tag{23d}$$

Eqs. (22) are similar to those that describe the physical fluxes. Hence they form a tri-diagonal system that can be solved with the bilinear concomitant providing the external boundary conditions. A check on the correctness of the results is possible via the relation

$$F_0(z) = \sum_{i=1}^{N} \int_{z_i}^{z_{i+1}} (\mathscr{F}_{0,i}(z), Q_0^i(z))\,\mathrm{d}z, \tag{24}$$

which calculates the physical flux. The formula is obtained from the left-hand side of Eq. (15a) as a sum over layers. Thus N_z locations where the flux is to be calculated will require N_z solutions. Since there are two coefficients per layer, the computational complexity will be of order $2N_z^2$. However, the tri-diagonal system of Eqs. (22a) and (22b) does not require $2N_z^2$ evaluations of the matrix of adjoint coefficients because z_0 is present only in the adjoint sources. In terms of an LU factorization of the adjoint coefficent matrix, this factorization need only be performed once.

While a complete analytic solution is possible, such an undertaking is not necessary for this discussion. Formulae (22a)–(23d) have been verified and reproduce the physical fluxes via (24) EXACTLY for both upwelling and downwelling diffuse fluxes using the general boundary conditions specified in Section 1. It should be noted that in formulas for the downwelling hemispherical flux, the direct beam contribution will be absent. Total flux requires that the direct beam be added after $F_1^-(z_1)$ is determined.

Although Eqs. (22) and (23) do not appear to have a simple physical interpretation, it is clear that $\mathscr{F}$ is an operator that acts on the source function as in (24) to yield the fluxes. Eq. (18) is the Greens function for the adjoint. It differs from the conventional Green's function by the way boundary conditions are used. The conventional Green's functions is obtained by simply replacing the spatially varying source with a delta function. The response is obtained by employing the same boundary conditions that are required for the solution of the two-stream fluxes. The adjoint flux or adjoint Greens function requires for its solution the physical fluxes emerging from the boundaries

of the medium (i.e. that the two-stream problem be solved). Hence the adjoint differential equation by itself cannot be used to determine the physical fluxes from the prescribed distribution of optical properties and physical boundary conditions.

The preceeding observations demonstrate that the adjoint is calculable for non-zero physical fluxes exiting the boundaries. The tri-diagonal solver can fail or may incur large numerical errors when the absorption and optical depth in the medium become large. The numerical behaviour of the global adjoint reflection and transmission functions (23a)–(23d) is worthy of note under these conditions. These functions are related to those of the physical flux by a simple exchange of parameters: $p_1 \to p_2$ and $p_2 \to p_1$. The consequence is that $\mathscr{R}$ and $\mathscr{T}$ can become negative, or exceed unity, and in the limit of complete absorption, all approach zero. The components of Eqs. (22a) and (22b) that do not contain $\mathscr{F}_{i+1}$ or $\mathscr{F}_{i-1}$ will be termed adjoint sources, as they are produced in response to the delta function stimulus and constitute the inhomogeneous solution to (18). This stimulus is applied at position z_0. The adjoint source will not be zero if z_0 does not lie within the (z_i, z_{i+1}) interval. As long as z_0 is less than z_i, the step functions will be unity, and the components of the exponential matrix $e^i_{l,m}$ will be present. These elements are unbounded and can lead to numerical instability.

Although the aforementioned analyses may suggest that there is no advantage to using the adjoint solution, the following considerations must be borne in mind: (a) the purpose of the adjoint is not to calculate the fluxes directly, but to be used as a device to define flux perturbations, (b) failure of the adjoint is caused by strong absorption. However, when absorption dominates, multiple scattering is minimal and the complexity of the radiative transfer problem for determining the fluxes is reduced significantly, as will be shown in Section 5, (c) when multiple scattering prevails in a medium, even if the latter is optically thick, tests show that the adjoint flux can be calculated without numerical difficulties. To complete this section, Eqs. (22a) and (22b) can be factored in terms of $\mathscr{R}(z)$, $\mathscr{T}(z)$ and the Heaviside function $H(z)$ in preparation for use in perturbations. The result is

$$\mathscr{F}^+_{0,i}(z, z_0) = \mathscr{A}^1_i \mathscr{T}^1_i(z) + \mathscr{A}^2_i \mathscr{R}^1_i(z) + (e^i_{2,2}(z - z_0)h^+ + e^i_{1,2}(z - z_0)h^-)H(z - z_0), \tag{25a}$$

$$\mathscr{F}^-_{0,i}(z, z_0) = \mathscr{A}^1_i \mathscr{R}^2_i(z) + \mathscr{A}^2_i \mathscr{T}^2_i(z) + (e^i_{2,1}(z - z_0)h^+ + e^i_{1,1}(z - z_0)h^-)H(z - z_0). \tag{25b}$$

One final shorthand notation will be employed in the development of the perturbation method by defining the adjoint source functions in (25a) and (25b) in terms of two functions, $\theta^1_i(z)$ and $\theta^2_i(z)$ given by

$$\theta^1_i(z) = (e^i_{2,2}(z - z_0)h^+ + e^i_{1,2}(z - z_0)h^-)H(z - z_0), \tag{25c}$$

$$\theta^2_i(z) = (e^i_{2,1}(z - z_0)h^+ + e^i_{1,1}(z - z_0)h^-)H(z - z_0). \tag{25d}$$

4. Perturbations

The prescription for calculating perturbations to the base state is contained in (1). It is now a matter of carrying through the integrations required by the first-order correction term:

$$\Delta F(z_0) = \langle \mathscr{F}_0, \Delta L F_0 \rangle. \tag{26a}$$

For multi-layer media, the integral implied in (26a) is replaced by the sum

$$\Delta F(z_0) = \sum_{i=1}^{N} \int_{z_i}^{z_{i+1}} (\mathscr{F}_{0,i}, \Delta L_i F_0(z))\, \mathrm{d}z. \tag{26b}$$

The integrand of the ith term may be expanded as follows:

$$\mathscr{F}_{0,i}(z)\Delta L_i F_{0,i}(z) = \delta\gamma_1^i\, \Pi_1^i(z) + \delta\gamma_2^i\, \Pi_2^i(z), \tag{26c}$$

where the expressions for the Π terms are:

$$\begin{aligned}
\Pi_1^i(z) = {} & \mathscr{A}_i^1 C_i^1(\mathscr{T}_i^1(z)R_i^2(z) - \mathscr{R}_i^2(z)T_i^1(z)) + \mathscr{A}_i^1 C_i^2(\mathscr{T}_i^1(z)T_i^2(z) - \mathscr{R}_i^2(z)R_i^1(z)) \\
& + \mathscr{A}_i^2 C_i^1(\mathscr{R}_i^1(z)R_i^2(z) - \mathscr{T}_i^2(z)T_i^1(z)) + \mathscr{A}_i^2 C_i^2(\mathscr{R}_i^1(z)T_i^2(z) - \mathscr{T}_i^2(z)R_i^1(z)) \\
& + C_i^1(\theta_i^2(z)T_i^1(z) - \theta_i^1(z)R_i^2(z)) + C_i^2(\theta_i^2(z)R_i^1(z) - \theta_i^1(z)T_i^2(z)) \\
& + \mathscr{A}_i^1 C_i^4 \mathscr{T}_i^1(z)\mathscr{X}_i(z) - \mathscr{A}_i^1 C_i^3 \mathscr{R}_i^2(z)\mathscr{X}_i(z) + \mathscr{A}_i^2 C_i^4 \mathscr{R}_i^1(z)\mathscr{X}_i(z) - \mathscr{A}_i^2 C_i^3 \mathscr{T}_i^2(z)\mathscr{X}_i(z) \\
& + C_i^3\theta_i^2(z)\mathscr{X}_i(z) - C_i^4\theta_i^1(z)\mathscr{X}_i(z),
\end{aligned} \tag{27a}$$

$$\begin{aligned}
\Pi_2^i(z) = {} & \mathscr{A}_i^1 C_i^1(\mathscr{R}_i^2(z)R_i^2(z) - \mathscr{T}_i^1(z)T_i^1(z)) + \mathscr{A}_i^1 C_i^2(\mathscr{R}_i^2(z)T_i^2(z) - \mathscr{T}_i^1(z)R_i^1(z)) \\
& + \mathscr{A}_i^2 C_i^1(\mathscr{T}_i^2(z)R_i^2(z) - \mathscr{R}_i^1(z)T_i^1(z)) + \mathscr{A}_i^2 C_i^2(\mathscr{T}_i^2(z)T_i^2(z) - \mathscr{R}_i^1(z)R_i^1(z)) \\
& + C_i^1(\theta_i^1(z)T_i^1(z) - \theta_i^2(z)R_i^2(z)) + C_i^2(\theta_i^1(z)R_i^1(z) - \theta_i^2(z)T_i^2(z)) \\
& + \mathscr{A}_i^1 C_i^4 \mathscr{R}_i^2(z)\mathscr{X}_i(z) - \mathscr{A}_i^1 C_i^3 \mathscr{T}_i^1(z)\mathscr{X}_i(z) + \mathscr{A}_i^2 C_i^4 \mathscr{T}_i^2(z)\mathscr{X}_i(z) - \mathscr{A}_i^2 C_i^3 \mathscr{R}_i^1(z)\mathscr{X}_i(z) \\
& + C_i^3\theta_i^1(z)\mathscr{X}_i(z) - C_i^4\theta_i^2(z)\mathscr{X}_i(z).
\end{aligned} \tag{27b}$$

The integrals of Π_1^i and Π_2^i required for the perturbations are associated with the base state. These integrals were evaluated manually and checked for algebraic correctness using *Mathematica* [10]. The transition operator is defined as

$$\Delta L_i = \begin{pmatrix} -\delta\gamma_1^i & \delta\gamma_2^i \\ -\delta\gamma_2^i & \delta\gamma_1^i \end{pmatrix}, \tag{28a}$$

where

$$\delta\gamma_1^i = \gamma_{1,\mathrm{f}}^i - \gamma_{1,\mathrm{b}}^i, \tag{28b}$$

$$\delta\gamma_2^i = \gamma_{1,\mathrm{f}}^i - \gamma_{2,\mathrm{b}}^i. \tag{28c}$$

The subscripts f and b in (28) refer to the final and base state, respectively. From (26c), it is seen that the first-order correction to the flux requires two multiplications and one addition per layer. Computational efficiency is achieved by calculating the base state only once at the required levels and storing the results in a database for subsequent use. The possibility of improving the accuracy of the first-order correction has been demonstrated in [1]. The correction, suggested by Box et al. [6] is

$$F(z) = F_0(z) \exp\left[\frac{-\Delta F(z)}{F_0(z)}\right] \tag{29}$$

and is applicable to the multi-layer case. A Taylor expansion of (29) recovers the first-order result.

The neglect of higher-order terms in (1) on the approximation can only be ascertained through numerical experimentation. Two issues that such experimentation may help resolve are those connected with the domain of applicability of (29) and to what extent conservation of energy may be violated. Such violation is not surprising even for the linear approximation, since only the first term of an infinite series in (1) is retained. For the application at hand, namely broadband computations in the presence of absorption, the perturbation method in concert with selection rules described in Section 5, has been found useful.

In the formulation presented, the perturbations only involve the attenuation matrix and not the sources. It is possible to incorporate changes in the latter that results in a physically more correct approach to the problem as indicated in Eq. (1) of Gabriel et al. [1]. The first term, $\langle \mathscr{F}_0 Q_f \rangle$, requires the source function of the final state. While this is easily formed, and an analytic expression for the ith layer can be written, the computational expense is high because every layer requires the evaluation of several coefficients and two exponentials that are functions of the final state. Because the results obtained without the inclusion of source term perturbations are promising, and because the evaluation of these terms adds significantly more computational burden, source term perturbations will not be pursued further.

5. Selection rules

The development of a rule-based algorithm to accelerate broadband radiative transfer calculations is an alternative to general purpose algorithms. For example, by examining the optical properties of atmospheres generated by the k-distribution method, a set of simple rules can be formulated that specify under what conditions full two-stream calculations are necessary, and under what conditions the direct beam solution is sufficient. This heuristic approach is a compromise that trades generality for speed with a possible reduction in accuracy. As such, facility in selecting the parameters described below that set the rules is, to some extent, a trial and error process.

Fig. 2 illustrates the optical properties of a typical midlatitude summer atmospheric profile for the cloudless sky calculated by the Fu and Liou k-distribution model [9]. The first column shows the variation in τ_s, τ_e and ω_0 as functions of altitude for the region of the spectrum extending from 50 000 to 14 500 cm^{-1} (band one). The second and third columns display the same information except that they represent data in the 14 500–7700 and 7700–5250 cm^{-1} (bands two and three, respectively). In band one, there are three radiatively important gases: nitrogen, oxygen and ozone. Nitrogen and oxygen give rise to molecular or Rayleigh scattering. Ozone is an absorbing gas. Therefore τ_s is equal to only the sum of the scattering cross sections of nitrogen and oxygen. The extinction, being the sum of the absorption and the scattering cross sections of the three gases, exhibits large variation due to the rapid change of the ozone absorption cross section with frequency.

With reference to Fig. 2, in the five sub-bands of band 1 that are circled, the single-scattering albedo is near unity ($\omega_0 > 0.975$) below 15 km and the extinction optical depths increase with decreasing altitude. The direct solar radiation suffers little attenuation above 15 km. Below this altitude, $\tau_s \approx \tau_e > 0.001$. These conditions make necessary the calculation of the diffuse flux. The threshold of 0.001 is indicated by the broken line in the first row of Fig. 2. In the remaining

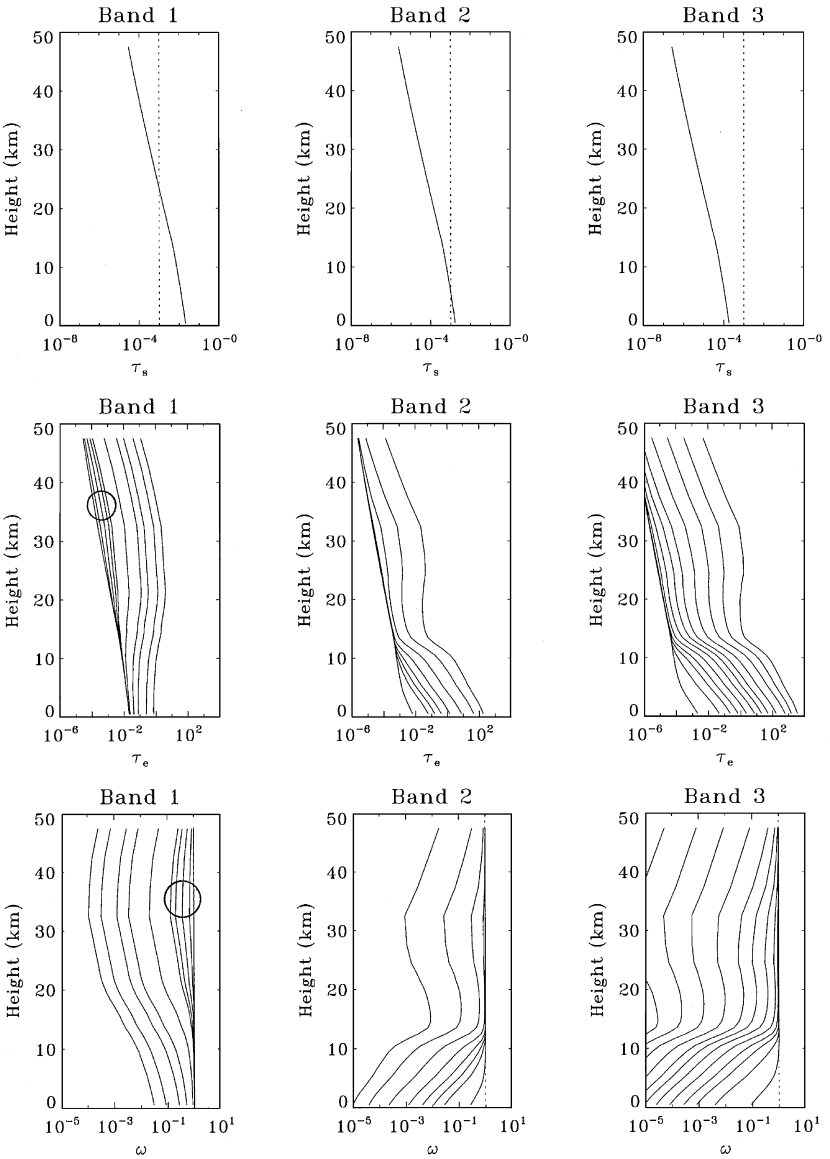

Fig. 2. Profiles of clear sky optical properties for the first three bands generated by the Fu and Liou k-distribution method. The plots show variations of the scattering optical depth, extinction optical depth and single-scattering albedo with altitude. The bundled curves in band one do not satisfy the threshold criteria used in the selection rules. The thresholds were set to $\omega_T = 0.975$ and $\tau_T^s = 0.001$ (vertical dotted line in the topmost plots). Selection rule violations occur in the lower atmosphere (below 10 km). The other curves in band one (or the sub-bands), satisfy the selection rule criteria, the need to perform the normally required, detailed multiple-scattering calculations is eliminated. In bands two and three the selection rule criteria are satisfied. For example, even though the single-scattering albedo can exceed that specified by ω_T above 6 km, the scattering optical depth is less than τ_T^s. Below 6 km, $\omega < \omega_T$. Thus, multiple scattering will not contribute to either the upwelling or downwelling fluxes significantly. The selection rules criteria are satisfied everywhere for bands four to six. The optical profiles for these bands are not shown.

sub-bands, ω_0 decreases while τ_e increases. The attendant reduction of τ_s diminishes the importance of multiple scattering, as the radiative transfer is dominated by absorption. In columns two and three, the active absorber is water vapour. The scattering cross sections decrease according to Rayleigh's law as the inverse fourth power of the wavelength. The scattering cross sections also decrease rapidly with altitude as may be seen from Fig. 2. The reflected and transmitted fluxes are then determined by the optically thin regime, wherein diffuse fluxes essentially rise from first order scattering and are dependent only on τ_s. Similar considerations apply also to band 3.

In the continuum bands where ω_0 is small (smallness here must be placed within the context of a specific application), the optical depth alone determines the accuracy of the fluxes (assuming that the asymmetry factor here is $g = 0$). In the limit of zero ω_0, there is no multiple scattering. As ω_0 increases from zero, the contribution by multiple scattering to the fluxes increases, reaching some asymptotic limit at a rate determined by τ_e. An examination of the optical properties of several atmospheres produced by the k-distribution shows that most of the contribution to the reflected fluxes is attributable to bands 1 and 2. These tendencies suggest that detailed radiative transfer calculations of fluxes need not be carried out for all bands. Instead, the direct beam will be the main contribution if the following conditions are met in an N layer medium:

$$\sum_{i=1}^{N} (\tau_i^s < \tau_T^s \cup \omega_i < \omega_T) = N. \tag{30}$$

The quantity in parentheses is a logical operation that returns unity if the condition indicated is true for the ith layer. Otherwise a zero is returned. Control over the logical condition is exerted by the selectable thresholds τ_T^s and ω_T. By summing the returned values over all layers, the optical properties can be catagorized. If the sum equals the number of layers, then the medium is either everywhere weakly scattering, everywhere strongly absorbing or both strongly absorbing and weakly scattering. These conditions disfavour full two-stream calculations to the extent determined by the thresholds. A single violation of the logical condition ensures that a full two-stream calculation will be performed. In all of the results to be presented, the scattering optical depth τ_T^s was set to 0.001 while ω_T varied as indicated.

To test the ideas just described, broad band fluxes computed using the selection rule method included into a two-stream model were compared against those obtained by a standard two-stream solver which computes a full two-stream solution for each of the 54 sub-intervals of the Fu and Liou k-distribution model [9] in a 30 layer atmosphere whose profile of optical properties were specified by the Colorado State University (CSU) global circulation model (GCM). This latter calculation is considered here as the benchmark, or "truth". The results of these calculations are presented in Fig. 3a. Illustrated are the upwelling and downwelling broadband fluxes and the flux divergences for clear sky, overhead sun and no surface reflection for two extremely different thresholds of ω_T. Fig. 3b. illustrates the differences (in W m^{-2}) between the true and approximate results. In general, the profiles of the fluxes and the flux divergences can be seen to be in excellent agreement.

Figs. 3c, d and e, f show the effect of introducing a Lambertian lower reflecting surface with an albedo, $R_g = 0.2$. In the case when full two-stream calculations are not required, the contributions

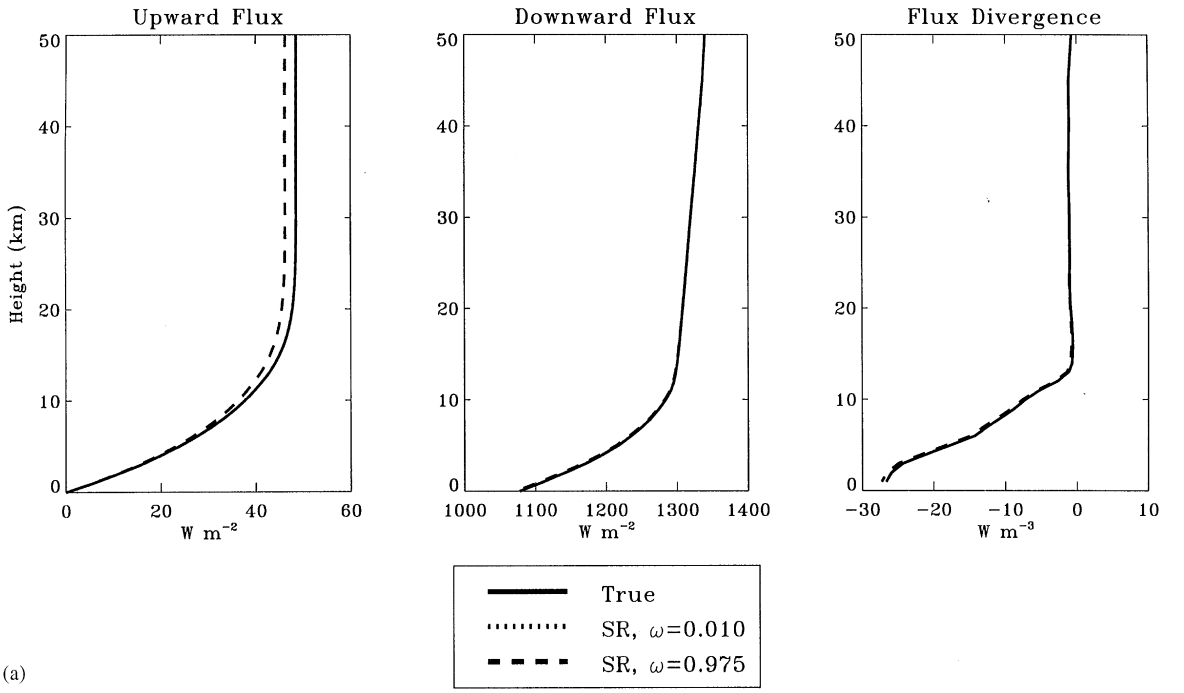

Fig. 3. (a) Three plots compare broadband upwelling and downwelling fluxes and the derived flux divergence calculated from full up multiple-scattering calculations to those calculated using selection rules in combination with a standard two-stream solver for the clear sky. The threshold for the scattering optical depth was set to 0.001. The thresholds for ω_T were set to 0.001 and 0.975. Zero diffuse radiation was incident on either the upper or lower boundaries and the sun was placed overhead. The atmosphere was specified by the CSU GCM and partitioned into 30 layers. (b) Absolute differences between upwelling fluxes, downwelling fluxes and flux divergences calculated from full up multiple-scattering

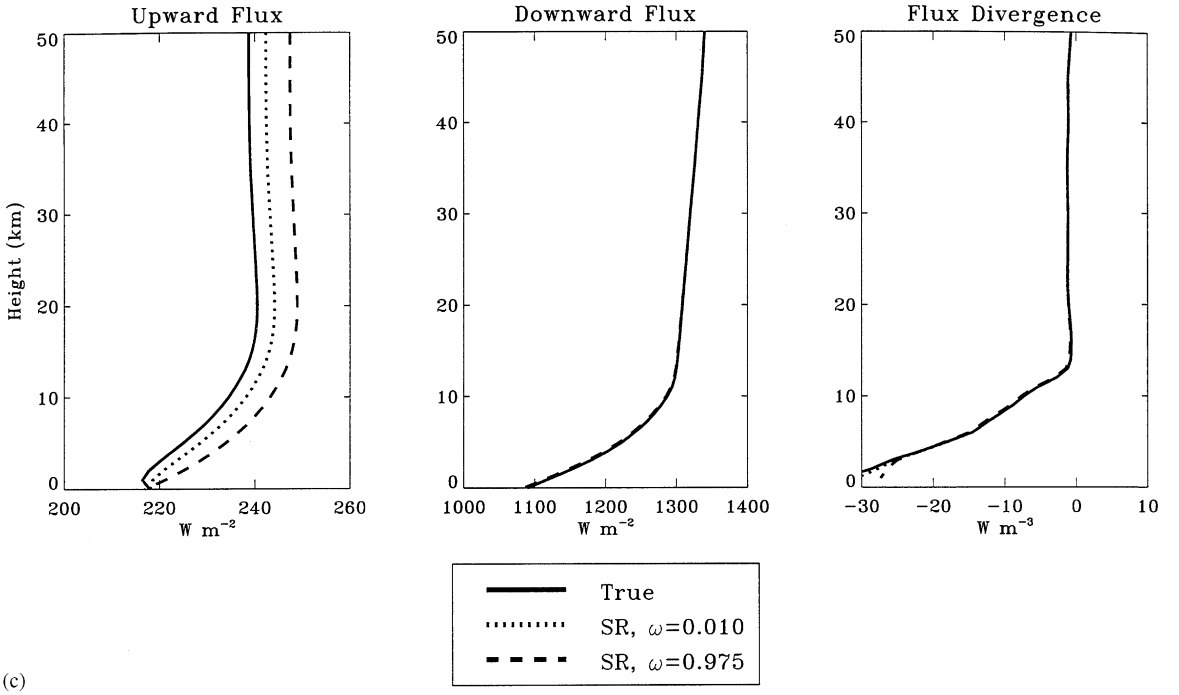

(c)

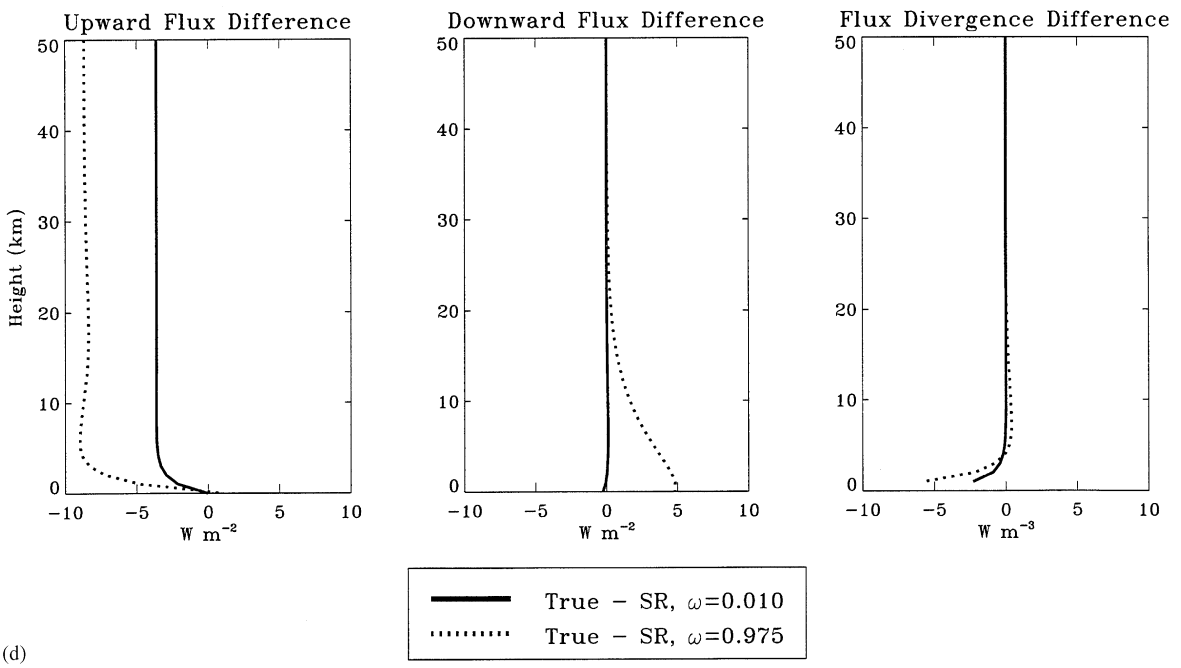

(d)

calculations (Fig. 3a) and those calculated from selection rules in combination with standard two-stream solvers. Thresholds and boundary conditions as in Fig. 3a. (c) As in Fig. 3a but with an isotropically reflecting lower surface with $R_g = 0.2$. (d) Absolute errors in the upwelling fluxes, downwelling fluxes and flux divergence computed from Fig. 3c. (e) As in Fig. 3a but with an isotropically reflecting lower surface with $R_g = 0.2$ and solar zenith angle of 60°. (f) Absolute errors in the upwelling fluxes, downwelling fluxes and flux divergence computed from Fig. 3e.

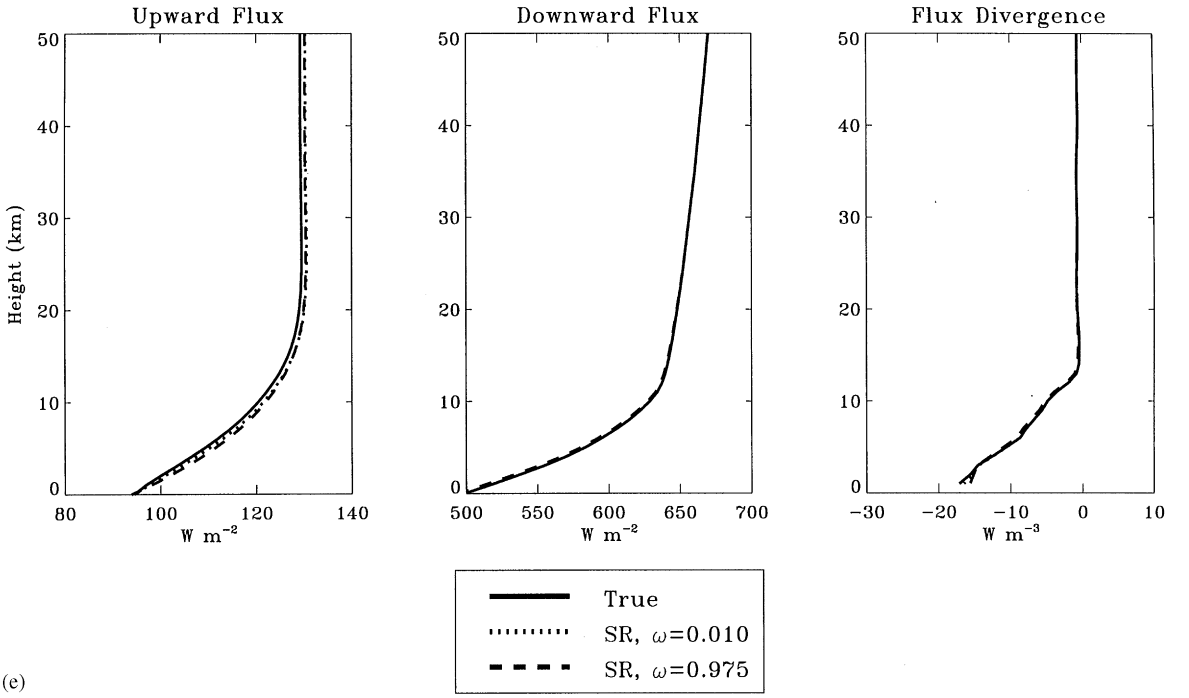

(e)

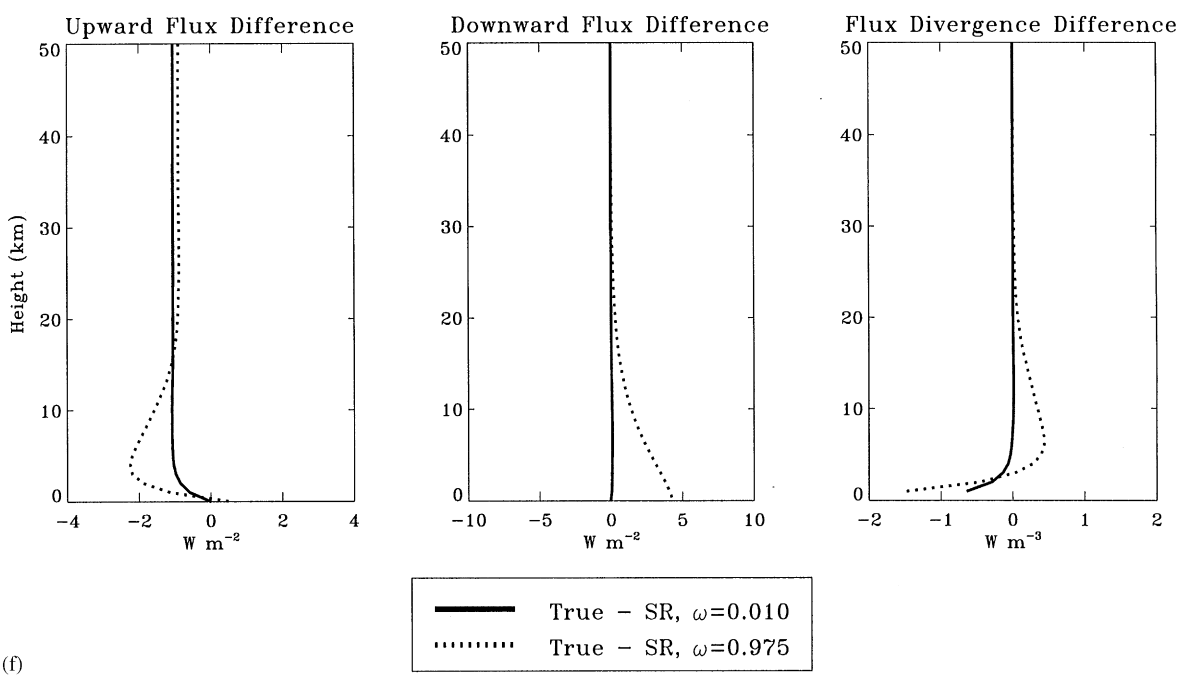

(f)

Fig. 3. (*continued*)

to the upwelling fluxes by surface reflection can be approximated in two ways. The first uses the direct radiation that impinges on the reflecting boundary, multiplies it by R_g, and then attenuates the result by weights $\mathrm{Exp}(-\tau_e^i)$ of the ith layer. The product of these weights yields the upwelling flux contribution at all positions throughout the medium.

The other approximation is cruder, faster and is based on the assumption that the gases (and clouds) in the lower atmosphere are strongly absorbing when the selection criterion applies. In this case, the magnitude of the direct beam is small. The extent of the attenuation is a strong function of the slant path of the solar radiation. The larger the solar zenith angle, θ_0, the smaller will be the magnitude of the direct beam. Therefore, the simplest correction is to ignore the attenuation of the reflected upwelling flux of the ith layer and to treat the reflected radiation as a constant throughout all the layers. Fig. 3c shows the accuracy that can be obtained when the sun is overhead ($\theta_0 = 0^\circ$). Fig. 3d shows the errors as a function of ω_T. Note that the broadband fluxes are calculated with accuracy, while the flux divergences at the lower boundary of the atmosphere exhibit some errors. The results obtained in Figs. 3e and f show how the errors in the flux divergences are reduced for large θ_0 (here $\theta_0 = 60^\circ$).

Other atmospheres studied yielded results comparable to those shown here. Of the 54 independent two-stream calculations that appear to be required, the selection rule method specified the need for only five diffuse calculations. The computational speed increase was just under a factor of 7. Changing ω_T from a value of 0.975–0.01 increased the number of calculations to 15 and decreased the computational gain to a factor of 3.5. The improvement in accuracy in the flux divergences is, however, negligible with this change in the albedo threshold. For the case of the overhead sun (or small solar zenith angles) and strongly reflecting lower surface, the smaller single-scattering threshold gives the greatest accuracy, as expected.

The selection rule method makes use of the extent of absorption and first-order scattering in an atmosphere to decide whether the diffuse flux is to be calculated. When clouds are present and the selection rule method applies, its effectiveness depends on the location of the clouds. If the clouds are situated within the lower atmosphere, the effect of gaseous absorption is to reduce the amount of direct radiation entering its boundaries in nearly all the sub-bands. Photons will not only be strongly absorbed by the interstitial gas, but by the cloud particles as well. At higher altitudes similar principles apply, however, the lower concentrations of absorbing gases increases the amount of energy reaching these clouds. Since the scattering optical depth of the cloud is much greater than that of the clear atmosphere, the determining factor that turns on or off full two-stream calculations is ω_T.

If ω_T is small, then small computational gains are realized, but high accuracy is attained. If ω_T is too large, then speed will be obtained, but the accuracy of the broadband fluxes and flux divergences eroded. Large errors in the flux divergences can be caused by small errors in the diffuse fluxes because the flux divergences are computed as differences between fluxes entering and leaving a layer divided by the layer thickness. Smaller values of ω_T may be required if accurate calculation of the flux divergences is the primary goal. The effect of reducing ω_T is to increase the accuracy of the computed internal fluxes. In applications that do not require heating rates such as in surface energy budgets, where only the surface flux is required, larger ω_T may be tolerable, if computational speed is important.

Broadband fluxes and flux divergences calculated by the selection rule method are compared to those computed from standard two-stream solver for an atmosphere containing a layered cirrus

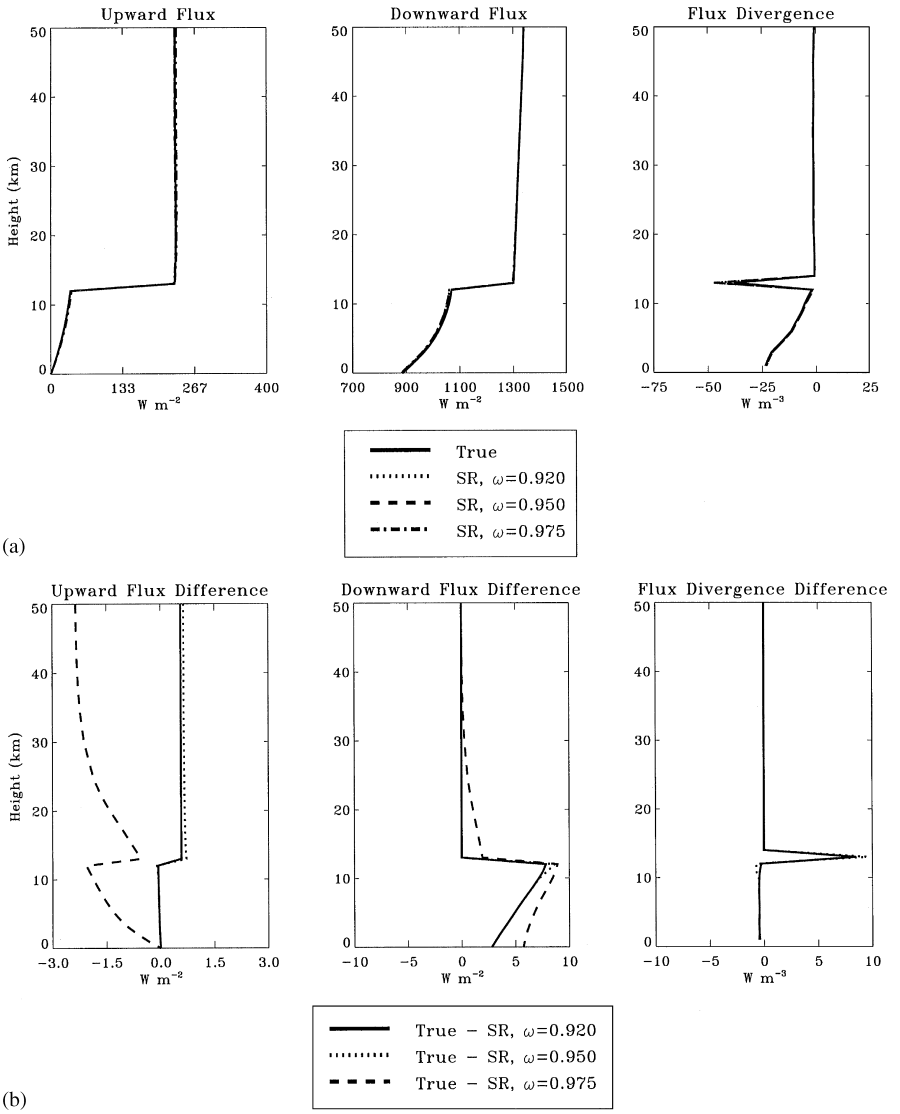

Fig. 4. (a) Comparison of broadband upwelling and downwelling fluxes and the derived flux divergence calculated from full up multiple scattering calculations to those calculated using selection rules in combination with a standard two-stream solver. A cirrus cloud extending from 12 to 13 km was embedded in the atmosphere used to calculate Fig. 1a. In band one the optical depth of this cloud was 3.7. The threshold for the scattering optical depth was set to 0.001. The thresholds for ω_T were set to 0.920, 0.950 and 0.975. Zero diffuse radiation was incident on either the upper or lower boundaries and the sun was placed overhead. (b) Absolute errors in the upwelling fluxes, downwelling fluxes and flux divergence computed from Fig. 4a.

cloud in Figs. 4a and b. In these tests, the surface was non-reflecting and θ_0 was 0°. The atmospheric profile was generated, as in the examples just discussed, by the CSU GCM. The cirrus cloud extends from 12 km (209 mb) to 13 km (179 mb) and has a scattering optical depth of 3.7 in band one. The extinction optical depth varies as a function of the wavelength due in part

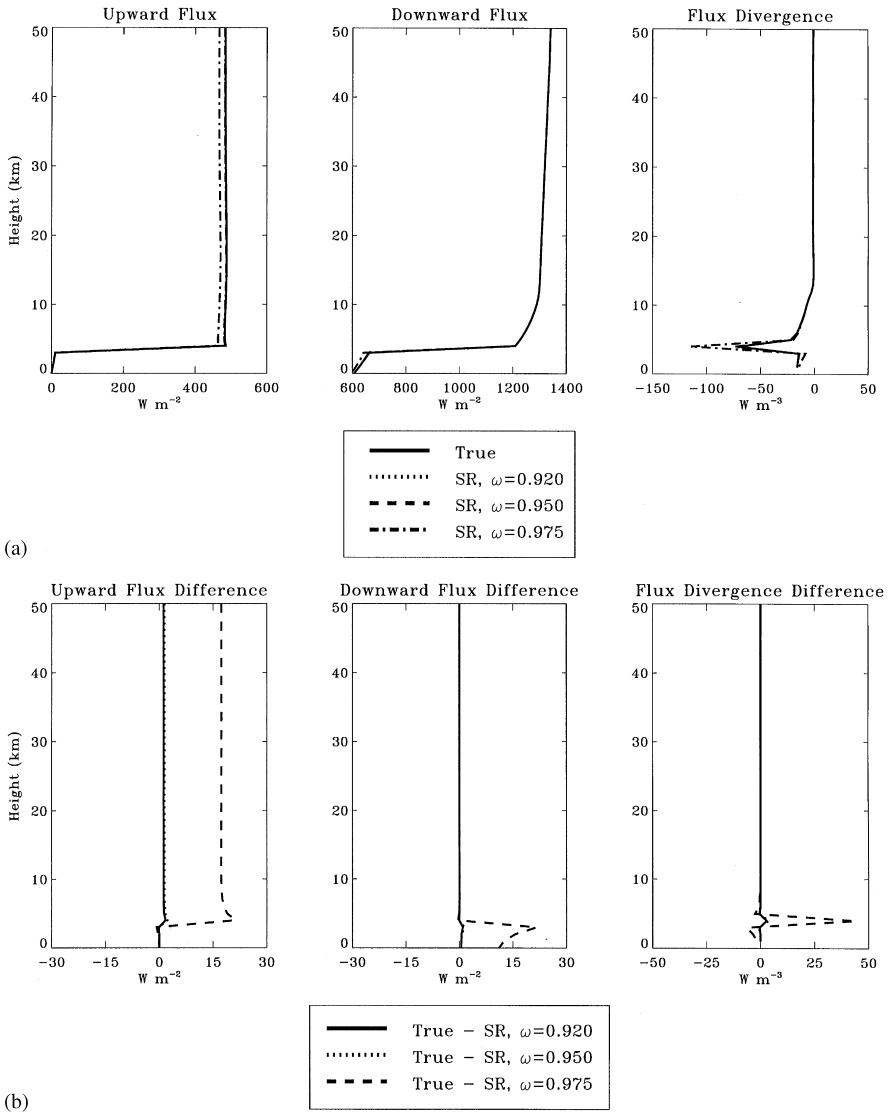

Fig. 5. (a) Comparison of broadband upwelling and downwelling fluxes and the derived flux divergence calculated from full up multiple scattering calculations to those calculated using selection rules in combination with a standard two-stream solver. A water cloud extending from 3 to 4 km was embedded in the atmosphere used to calculate Fig. 1a. In band one the optical depth of this cloud was 3.7. The threshold for the scattering optical depth was set to 0.001. The thresholds for ω_T were set to 0.920, 0.950 and 0.975. Zero diffuse radiation was incident on either the upper or lower boundaries and the sun was placed overhead. (b) Absolute errors in the upwelling fluxes, downwelling fluxes and flux divergence computed from Fig. 4a.

to the presence of water vapour and ozone, hence is sub-band dependent. The asymmetry factor is also sub-band dependent and is defined as an appropriate mixture of Rayleigh and cloud particle asymmetry factors. Of the normally required 54 radiative transfer calculations, 32 or 29 full two-stream calculations were performed using $\omega_T = 0.920$ and 0.975, respectively, with

corresponding compuational gains of 1.68 and 1.84. It was surprising that when $\omega_T = 0.95$, the number of full two-stream calculations was equal to that of the $\omega_T = 0.920$ threshold.

Similar results for low-level water clouds are presented in Figs. 5a and b. The setup is for a single-layer cloud extending between 3 to 4 km or between 710 and 628 mb, overhead sun and no ground reflections. The accuracy of the fluxes increases with decreasing ω_T as is also evident from Fig. 5b. The computational gains are 2.13, 2.42 and 3.29 corresponding to ω_T values of 0.920, 0.950 and 0.975, respectively. Fluxes are calculated accurately for all values of ω_T (the largest relative error in the upwelling flux is 3%, in the downwelling flux it is under 2%) while the flux divergence for $\omega_T = 0.975$ suffers an error exceeding 30%. Thus the flux divergence is calculated poorly, but fluxes at the boundaries may be of acceptable accuracy for certain applications. The inclusion of surface reflections did not affect the accuracy of the computed fluxes perceptibly. Increasing the solar zenith angle to 60° also did not significantly change the nature of the comparisons.

6. Adjoint perturbations with selection rules

This section describes the adjoint perturbation method used in conjunction with selection rules. These computational acceleration methods compliment each other: selection rules as defined in this paper cannot account for multiple scattering, while stability considerations restrict the perturbation approximation to media characterized by a high degree of multiple scattering. It is however the selection rule method that orchestrates the broadband calculation. Even so, there is an issue that concerns the optimal selection of the base states. Given that the selection specifies the sub-bands where a full multiple-scattering treatment is required, it is neccessary to select perhaps one or two of these sub-bands to carry out the perturbations for that (entire) band. It has been observed that the attainable accuracy depends on the selection of base states. In the case of the clear sky, that dependence is weak. For the cloudy sky, it may be significant. To explore some of these issues, this section first shows the dynamic range of the perturbations that can be accommodated followed by an example application where broadband calculations are performed for the continuum.

Table 2a depicts the optical properties of a hypothetical, vertically inhomogeneous 19 layer medium used to produce the results discussed below. The benchmark fluxes and the perturbed fluxes are given in Table 2b. Calculations were performed for overhead sun and a surface reflection of 0.2. No diffuse radiation entered the upper boundary, and the incident, direct radiation was set to unity. The scale factors indicated, multiply both the extinction and scattering coefficients. Scale factors of unity define the base state. For example, when the scale factor is 1.25, the base state extinction and scattering coefficients are multiplied by that factor, and the adjoint perturbation calculates the fluxes for this new optical profile from the base state. The asymmetry factors of the base state were maintained in the perturbations.

6.1. Monochromatic flux calculations with adjoint perturbations

To begin this discussion, it will be observed that the upwelling flux in layer 2 is negative (see Table 2b with scale factor = 1.0). This is not an error, but occurred as a result of the violation of the

Table 2a

Layer	z_l	z_h	σ_e	σ_s	g
01	00.0	01.0	0.20000	0.19000	0.00
02	01.0	02.0	1.00000	0.09000	0.85
03	02.0	03.0	0.20000	0.19000	0.00
04	03.0	04.0	0.15000	0.14900	0.00
05	04.0	05.0	0.15000	0.14900	0.00
06	05.0	06.0	0.15000	0.14900	0.00
07	06.0	07.0	3.00000	2.99999	0.85
08	07.0	08.0	0.15000	0.14999	0.00
09	08.0	09.0	0.15000	0.14999	0.00
10	09.0	10.0	0.15000	0.14999	0.00
11	10.0	11.0	0.10000	0.09999	0.00
12	11.0	12.0	0.15000	0.14999	0.00
13	12.0	13.0	0.10000	0.09999	0.00
14	13.0	14.0	0.10000	0.09999	0.00
15	14.0	16.0	0.05000	0.04999	0.00
16	15.0	16.0	0.05000	0.04999	0.00
17	16.0	17.0	0.05000	0.04999	0.00
18	17.0	18.0	0.05000	0.04999	0.00
19	18.0	20.0	0.05000	0.04999	0.00

Optical properties of an artificial 19 layer atmosphere containing two clouds in layers 2 and 7. This data set constitues the base state for the adjoint perturbations used to compute the fluxes in Table 2b and to compute fluxes in Fig. 7. Parameters z_l and z_h specify the position of the lower and upper levels of the ith layer.

Table 2b

z	F^+_{true}	F^+_{pert}	F^-_{true}	F^-_{pert}
Scale factor = 0.50				
19.999990	0.36110	0.32420	1.00000	1.00000
18.000010	0.34935	0.32303	0.99884	0.98823
17.000010	0.34325	0.32158	0.99739	0.98211
16.000010	0.33700	0.31959	0.99541	0.97586
15.000010	0.33061	0.31708	0.99291	0.96946
14.000010	0.31742	0.31064	0.98647	0.95626
13.000010	0.30370	0.30244	0.97827	0.94253
12.000010	0.28948	0.29264	0.96847	0.92831
11.000010	0.26727	0.27527	0.95111	0.90609
10.000010	0.25192	0.26212	0.93795	0.89073
09.000010	0.22810	0.24030	0.91614	0.86690
08.000010	0.20340	0.21631	0.89214	0.84220
07.000010	0.17789	0.19044	0.86627	0.81668
06.000010	0.11567	0.11852	0.79435	0.75445
05.000010	0.08646	0.08561	0.76094	0.72457
04.000010	0.05682	0.05205	0.72686	0.69430
03.000010	0.02675	0.01794	0.69222	0.66366
02.000010	− 0.01154	− 0.02591	0.64281	0.62022
01.000010	0.01788	0.02171	0.25163	0.32475
00.000010	0.00000	0.00000	0.22661	0.30439

Table 2b (*continued*)

z	F^+_{true}	F^+_{pert}	F^-_{true}	F^-_{pert}
Scale factor = 1.00				
19.999990	0.54263	0.54263	1.00000	1.00000
18.000010	0.53214	0.53214	0.98947	0.98947
17.000010	0.52604	0.52064	0.98334	0.98334
16.000010	0.51939	0.51939	0.97668	0.97668
15.000010	0.51224	0.51224	0.96950	0.96950
14.000010	0.49648	0.49648	0.95372	0.95372
13.000010	0.47897	0.47897	0.93619	0.93619
12.000010	0.45968	0.45968	0.91705	0.91705
11.000010	0.42853	0.42853	0.88570	0.88570
10.000010	0.40606	0.40606	0.86322	0.86322
09.000010	0.37029	0.37029	0.82743	0.82743
08.000010	0.33234	0.33234	0.78946	0.78946
07.000010	0.29252	0.29252	0.74962	0.74962
06.000010	0.17874	0.17874	0.63581	0.63581
05.000010	0.13244	0.13244	0.58810	0.58810
04.000010	0.08561	0.08561	0.54002	0.54002
03.000010	0.03830	0.03830	0.49164	0.49164
02.000010	− 0.02112	− 0.02112	0.42362	0.42362
01.000010	0.01904	0.01904	0.09818	0.09818
00.000010	0.00000	0.00000	0.08552	0.08552
Scale factor = 1.50				
19.999990	0.64902	0.68825	1.00000	1.00000
18.000010	0.64440	0.67155	0.99531	0.98322
17.000010	0.64023	0.66234	0.99110	0.97397
16.000010	0.63494	0.65260	0.98577	0.96419
15.000010	0.62860	0.64234	0.97940	0.95389
14.000010	0.61310	0.62038	0.96385	0.93189
13.000010	0.59426	0.59655	0.94497	0.90813
12.000010	0.57255	0.57134	0.92323	0.88277
11.000010	0.53547	0.53069	0.88611	0.84210
10.000010	0.50823	0.50203	0.85884	0.81340
09.000010	0.46426	0.45695	0.81483	0.76828
08.000010	0.41724	0.40970	0.76777	0.72100
07.000010	0.36778	0.36057	0.71828	0.67184
06.000010	0.21770	0.21887	0.56817	0.53012
05.000010	0.16201	0.16366	0.51036	0.47287
04.000010	0.10605	0.10798	0.45260	0.41546
03.000010	0.04985	0.05187	0.39493	0.35792
02.000010	− 0.01965	− 0.01794	0.31464	0.27749
01.000010	0.00508	0.00376	0.03123	− 0.00413
00.000010	0.00000	0.00000	0.02528	− 0.00854

This table explores the dynamic range that the adjoint perturbation method can accomodate for the base-state profile given in Table 2a for selected scale factors. True upwelling fluxes F^+_{true} and downwelling fluxes F^-_{true} are compared to those calculated by the adjoint perturbation method F^+_{pert} and F^-_{pert}, repectively, when both the extinction coefficients σ_e and the scattering coefficients are multiplied everywhere by the indicated scalefactor. The boundary conditions specify no surface reflections and no diffuse flux entering the upper boundary. The solar zenith angle was set to 0 degrees.

positivity requirements described in Section 3 for that layer. This may bring into question the accuracy of the base-state fluxes, since these are obtained from a coupled system of equations, and the manner by which errors are distributed is unknown. But it is not the absolute accuracy of the base-state fluxes that is the focus of this section, rather the focus is on comparing the approximated fluxes to the true fluxes. The negative flux result will not affect the comparisons because the adjoint coefficients reproduce the physical fluxes exactly at all locations in the medium, even if they are negative. As long as the two-stream model entering into the calculation of the adjoint and physical fluxes is identical, the computed fluxes will be identical. Fig. 6a shows the absolute differences between the true fluxes and those calculated using linear and exponential corrections to the base-state fluxes. The flux at the top of the atmosphere was set to one unit. The exponential corrections were calculated by using Eq. (29). Also, shown are the true flux divergences and their absolute differences from those calculated using the aforementioned corrections to the base-state fluxes. The upwelling fluxes appear to be calculated accurately (with errors lying between $+0.06$ and -0.06) for scale factors spanning the range 0.50–1.75. A more quantiative assesment can be made by examining the relative errors shown in Fig. 6b. Perturbations between 0.85 and 1.12 cause the upwelling fluxes calculated by linear corrections to the base state to be in error by less than 10%. In fact, the situation is much better than this because the true fluxes below 6 km are less than 0.1. By comparison, exponential corrections to base-state fluxes cause the error to be less than 10% below the region where the cloud is situated for scale factors in the range 0.25–0.85. For the upwelling fluxes, the linear correction works well when the deviations from the base state are small or if the medium is everywhere optically thin, in which case large perturbations can be accomodated. Similar considerations apply to exponential corrections, except that the range spanned by the perturbations in the optical properties where good accuracy (less than 10%) is obtainable, is extended. Downwelling fluxes are calculated more accurately than the upwelling fluxes for both linear and exponential corrections. This is consistent with the findings reported by Gabriel et al. [1] for the single-layer medium. The linear correction is more accurate when the optical thickness of the layers constituting the medium is reduced. The exponential correction extends greatly the range of the perturbations, favouring increasing departures in the optical depth from the base state. For the flux divergences, only differences between the benchmarks and those derived by the linear and exponential corrections to the base state fluxes are shown. The reason for not showing the relative errors is that the plots appear very busy due to the possibility of the flux divergences going negative, complicating interpretations. In any case, the significance of accuracy in the flux divergences becomes a moot point, only resolvable by global circulation or single-column models of the atmosphere.

A final example that explores the differences between linear and exponential corrections to the base-state fluxes is illustrated in Fig. 7. Here, the fluxes were calculated using the data in Table 2a. Instead of perturbing both the extinction and scattering coefficients by the same, constant scale factor, the extinction coefficient was left unchanged and only the scattering coefficient of layer two was multiplied by the scale factors shown. This hypothetical example introduces a large amount of absorption in the final-state optical profile. This tests the accuracy of the physical fluxes calculated by the adjoint perturbation method when the base state is characterized by weak absorption and shows how errors in fluxes propagate to the other layers. The relative errors in the upwelling flux are less than 10% at all locations for linear corrections to the base-state fluxes when the scattering coefficient is multipled by scale factors less than three (the base state scattering

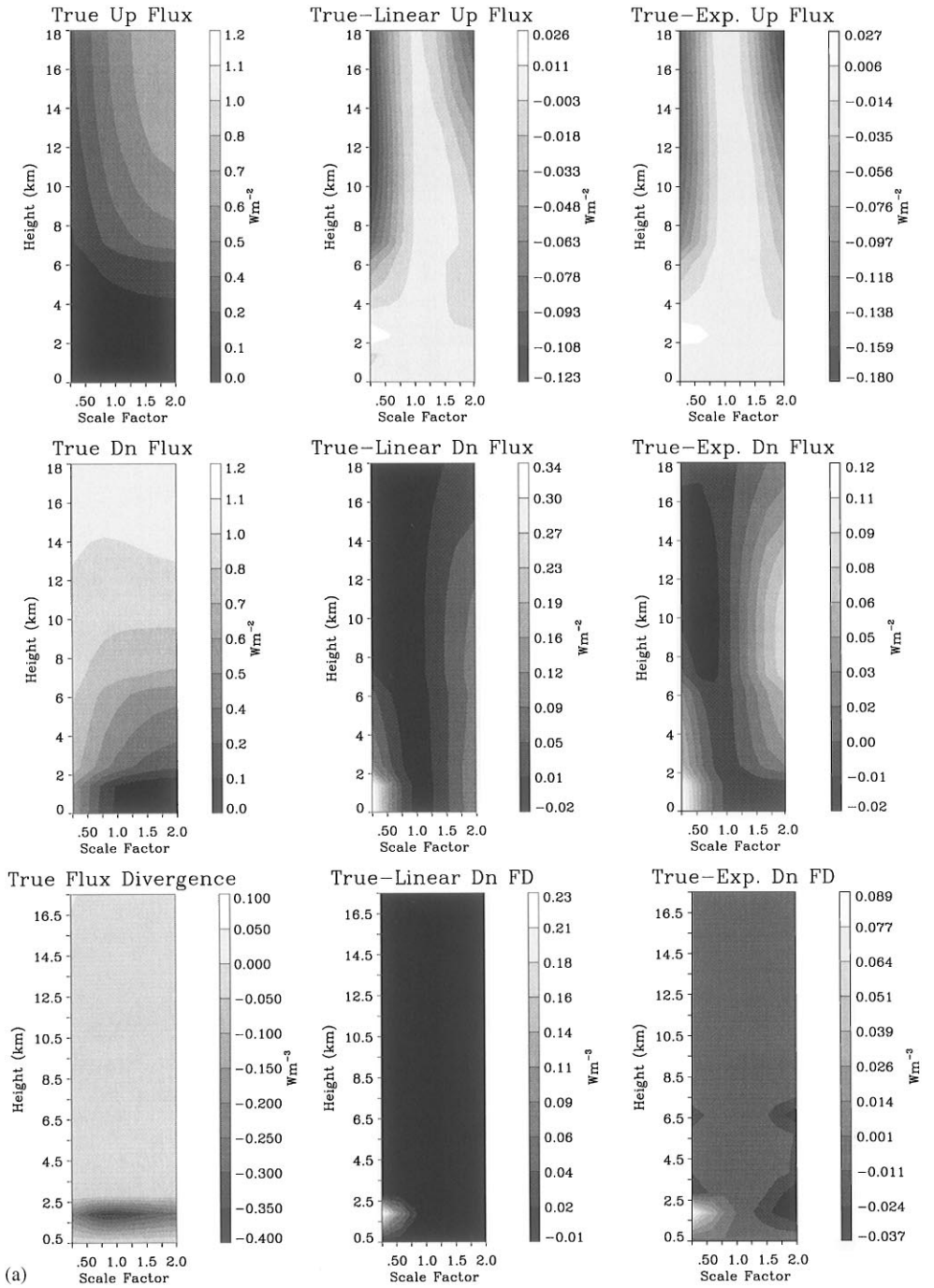

Fig. 6. (a) These graphics explore the sensitivity of fluxes calculated by the adjoint perturbation method to large departures from the base-state optical properties. The sensitivity is expressed in terms of an absolute error, calculated as the difference between fluxes obtained from a standard two-stream solver and fluxes computed from the adjoint perturbation method. Also shown are the exponential corrections to the base state fluxes discussed in the text. The scale

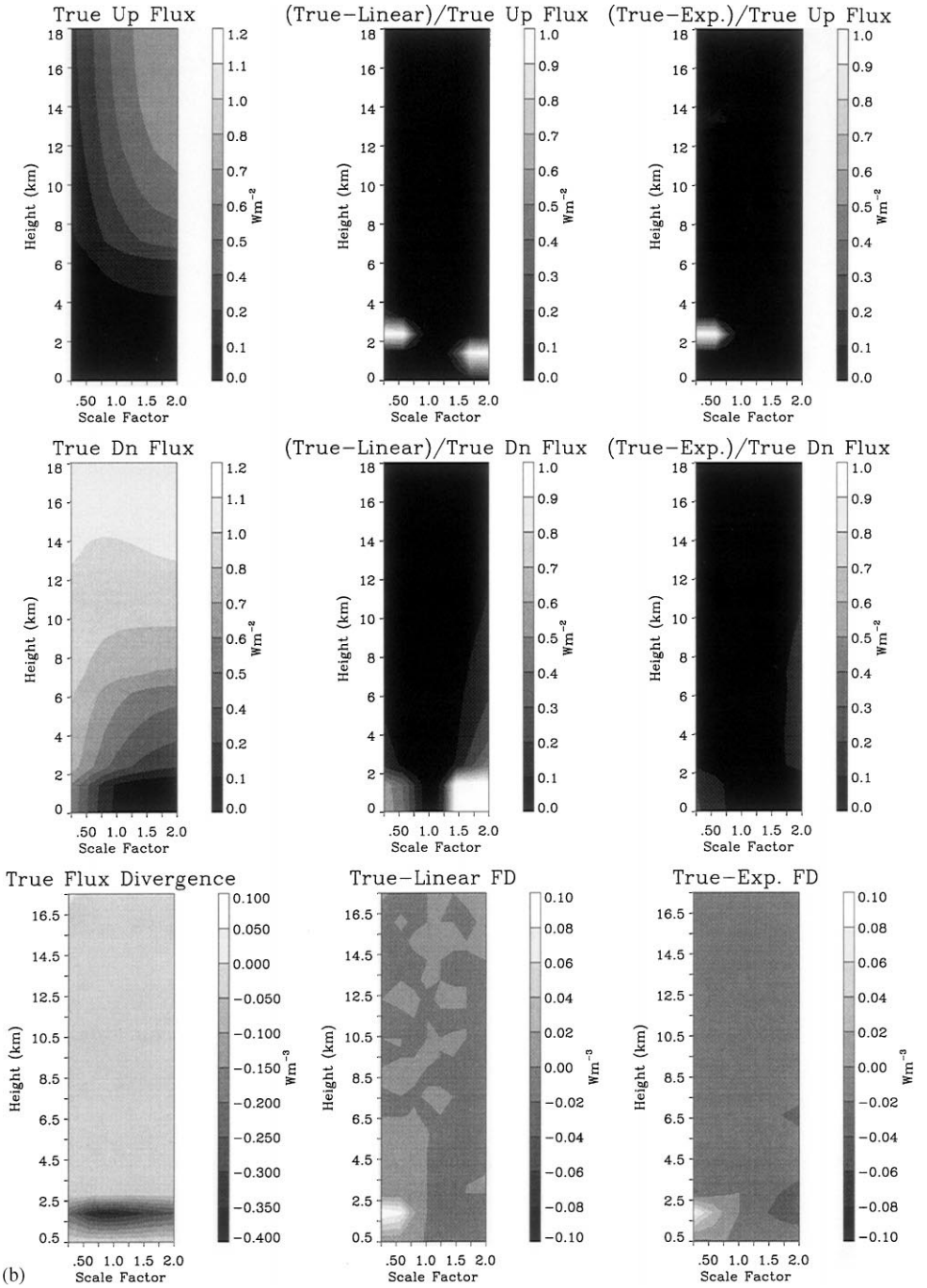

(b)

factor that labels the ordinate indicates the multiplicative factor applied to both the exinction and scattering coefficients. (b) Comparison of the relative errors in the upwelling and downwelling fluxes computed from Fig. 6a for linear and exponential corrections to the base-state fluxes.

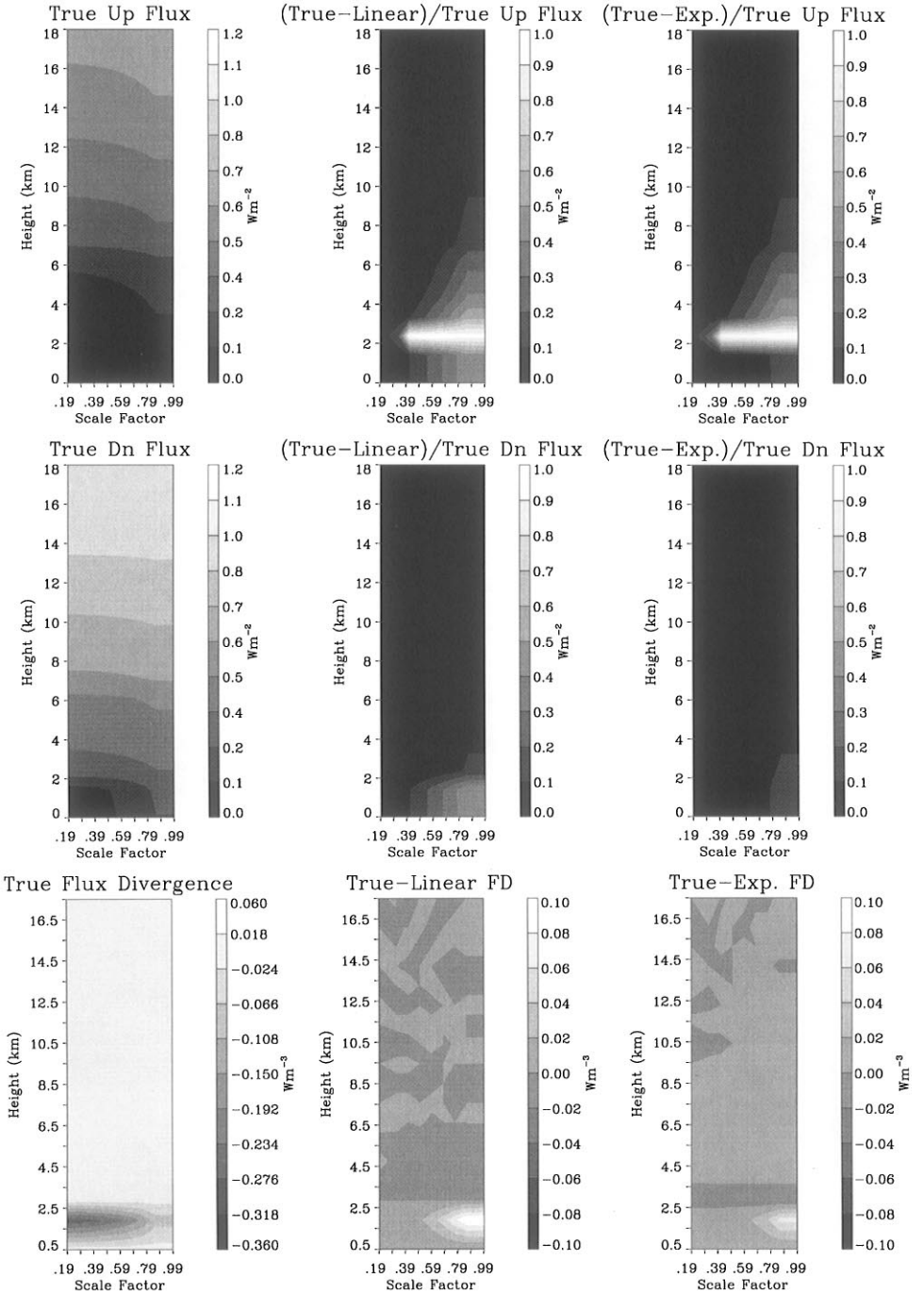
True Up Flux
(True−Linear)/True Up Flux
(True−Exp.)/True Up Flux
True Dn Flux
(True−Linear)/True Dn Flux
(True−Exp.)/True Dn Flux
True Flux Divergence
True−Linear FD
True−Exp. FD
Height (km)
Scale Factor
.19 .39 .59 .79 .99
Wm-2
Wm-3

coefficient for layer 2 is 0.09). The exponential correction to the base-state upwelling fluxes yields results that are similar to those using linear corrections. However, the exponential corrections constrain the propagation of errors. The improvement is dramatic for the downwelling fluxes, where the relative errors fall under 10% everywhere for perturbations exceeding a factor of eight.

6.2. Synthesis of broadband fluxes

Broadband calculations performed for the clear sky, which use both selection rules and adjoint perturbations, have been performed on test cases using optical profiles identical to those used in the calculation of Figs. 3–5. The selection rule threshold for ω_T was set to 0.975, requiring a total of five full radiative transfer calculations, all in band one (see Section 4). Numerical experiments showed that broadband fluxes and flux divergences exhibit a small sensitivity to the base state. The result of one experiment is illustrated in Figs. 8a and b for overhead sun and an absorbing surface. Two comparisons against the benchmarks are shown: fluxes calculated by selection rules in combination with the adding method and fluxes computed by combining the adjoint perturbations with the selection rule method. In all cases the results are in good agreement. Increasing the surface reflection to 0.2 (Figs. 9a and b) but maintaining the solar zenith angle ($\theta_0 = 0^\circ$) yields slightly diminished accuracy. The quantity most affected is the upwelling flux. It will be observed that the selection rules method is slightly more accurate than when it is used with adjoint perturbations. In fact, errors in the fluxes computed using the latter technique are attributable to the selection rule method and the way it treats surface reflections as seen in Figs. 10a and b which applies to the case of $\theta_0 = 60^\circ$. Errors in the computed fluxes for the case of an oblique sun are substantially smaller than in the overhead sun case for the reasons discussed in Section 4. Errors introduced by the adjoint perturbations are comparable to or smaller than those introduced by the selection rule method operating in combination with the adding method. Although only three calculations involving perturbations are required for the case given, the bands where the perturbations are performed contain a great deal of energy and thus contribute significantly to the broadband fluxes.

7. Summary and conclusions

This paper describes computationally efficient techniques for solving two-stream spectral and broadband fluxes in multi-layered media. The methods developed involve a perturbation approach that requires a solution to the adjoint of the two-stream equation and a selection rule method that determines when multiple-scattering solutions are required. The development of the adjoint

Fig. 7. These graphics explore the sensitivity of fluxes calculated by the adjoint perturbation method to large local departures from the base-state optical properties. The atmospheric profile given in Table 2a is perturbed only in the second layer by maintaining the given extinction coefficient but multiplying the scattering coefficient by the indicated scale factor. Sensitivity is expressed in terms of a relative error. Also shown are the exponential corrections to the base-state fluxes discussed in the text. The scale factor that labels the ordinate indicates the multiplicative factor applied to both the exinction and scattering coefficients.

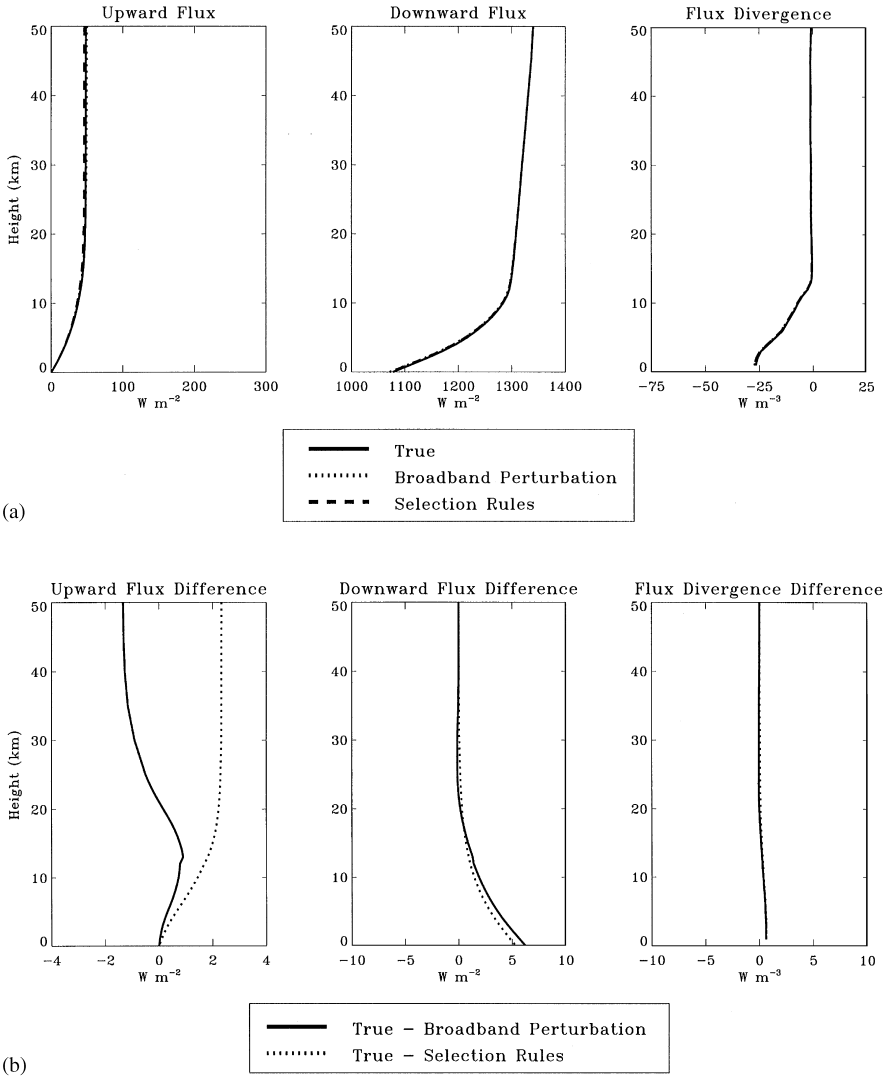

Fig. 8. (a) Broadband fluxes for the clear sky calclulated by the adjoint perturbation method in combination with selection rules and selection rules in combination with standard flux solvers. The threshold $\omega_T = 0.975$. No diffuse radiation was incident on the boundaries of the atmosphere and the solar zenith angle was 0° or overhead sun. The optical profiles of the base state were supplied by the CSU GCM. (b) Absolute differences between the true and approximate broadband fluxes calculated from Fig. 8a.

perturbation method proceeds in three stages: (1) The two-stream equations are solved analytically. The solution presented in this paper differs from that given by the standard adding approach in that the fluxes can be calculated continuously at any point within the medium, not only at layer interfaces. This formulation of fluxes is required for the evaluation of the perturbation integrals. (2) The adjoint solution, which constitutes a part of the base state, is obtained. This is an operator that has no simple physical interpretation. Unlike Greens function, the adjoint requires the

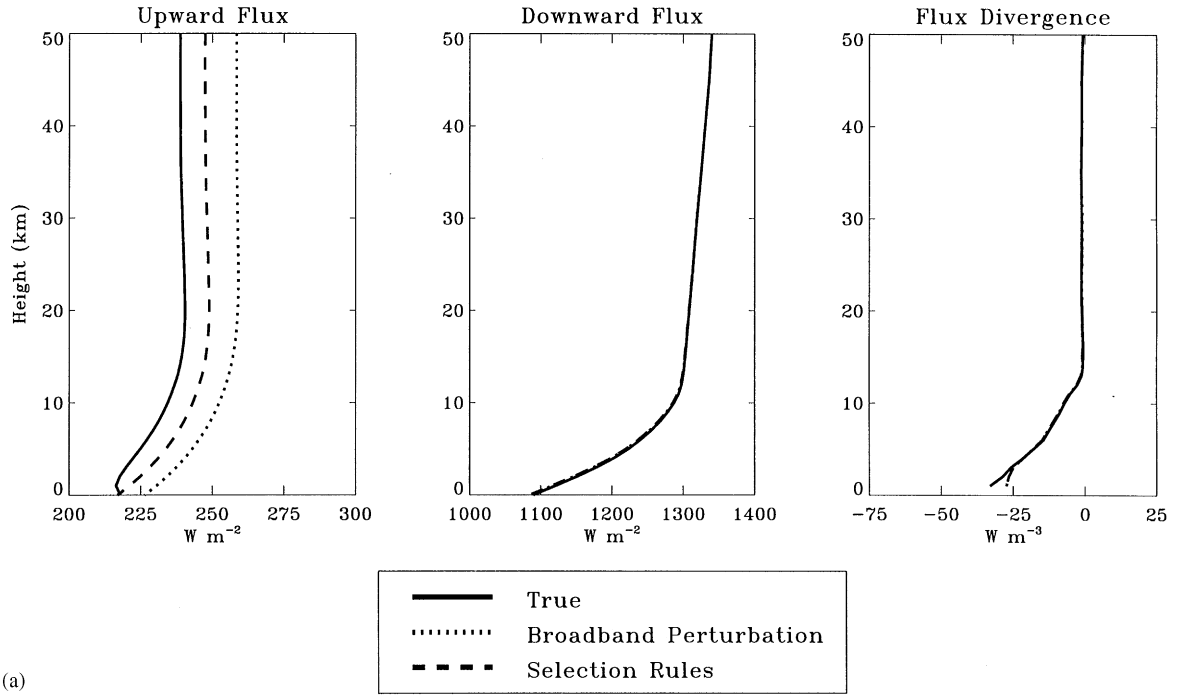

(a)

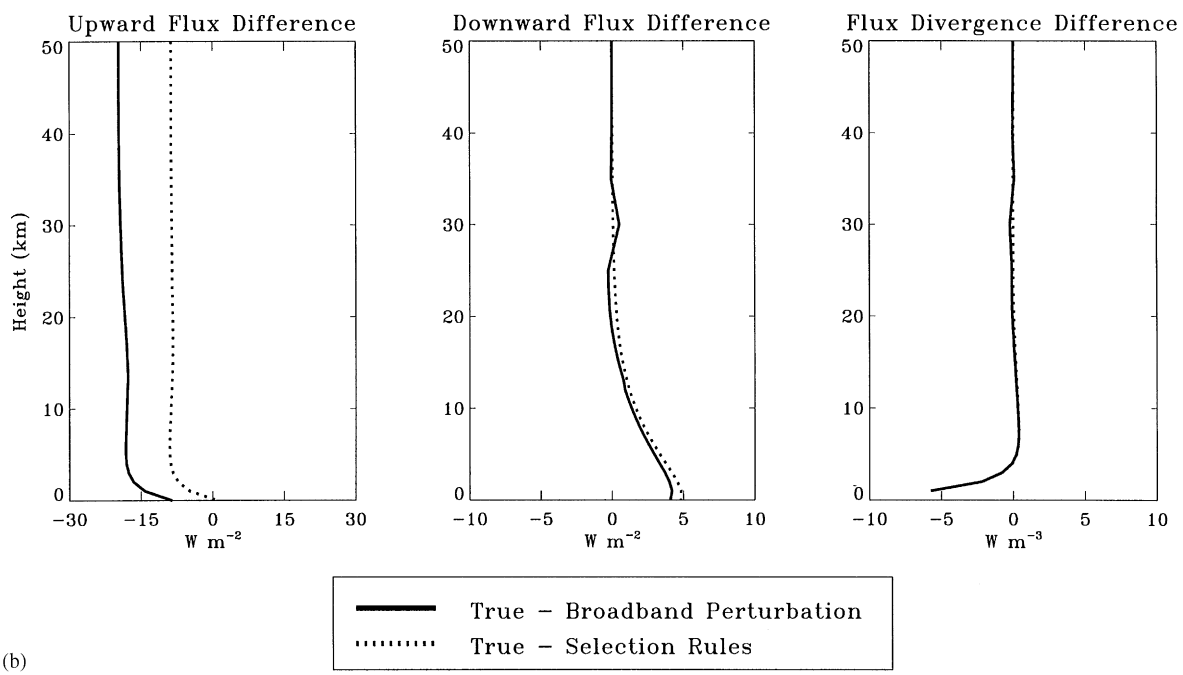

(b)

Fig. 9. (a) As in Fig. 8a with the exception that the underlying surface albedo was 0.2. (b) Absolute errors in broadband fluxes computed from Fig. 9a.

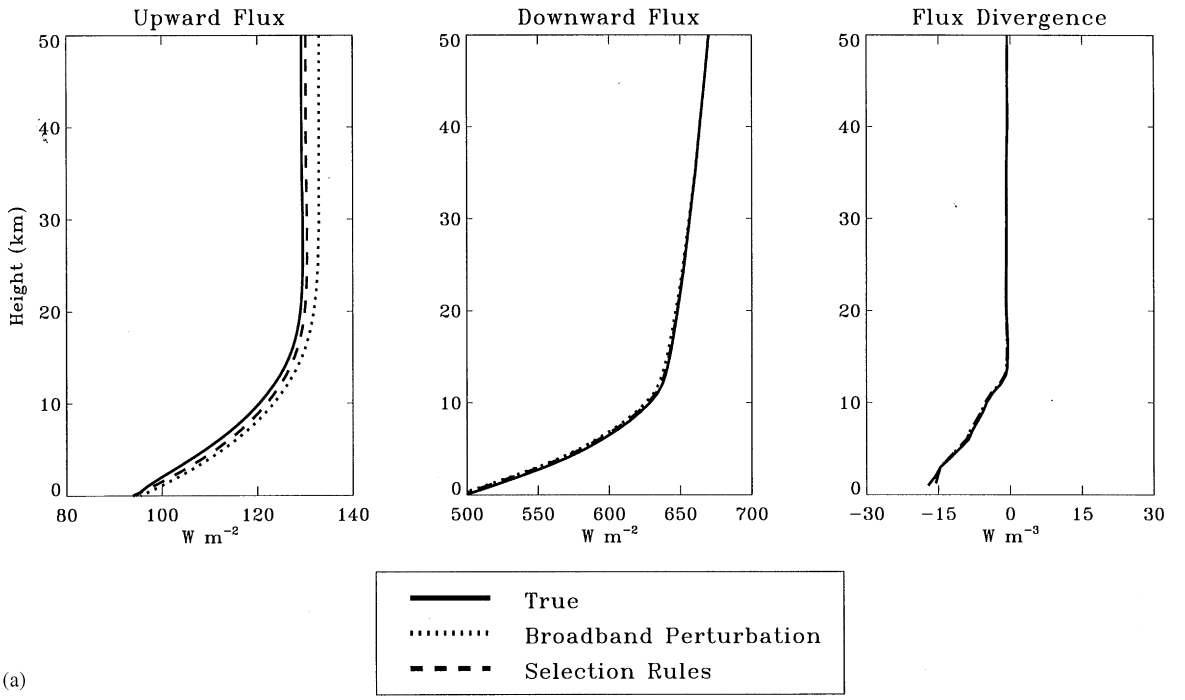

(a)

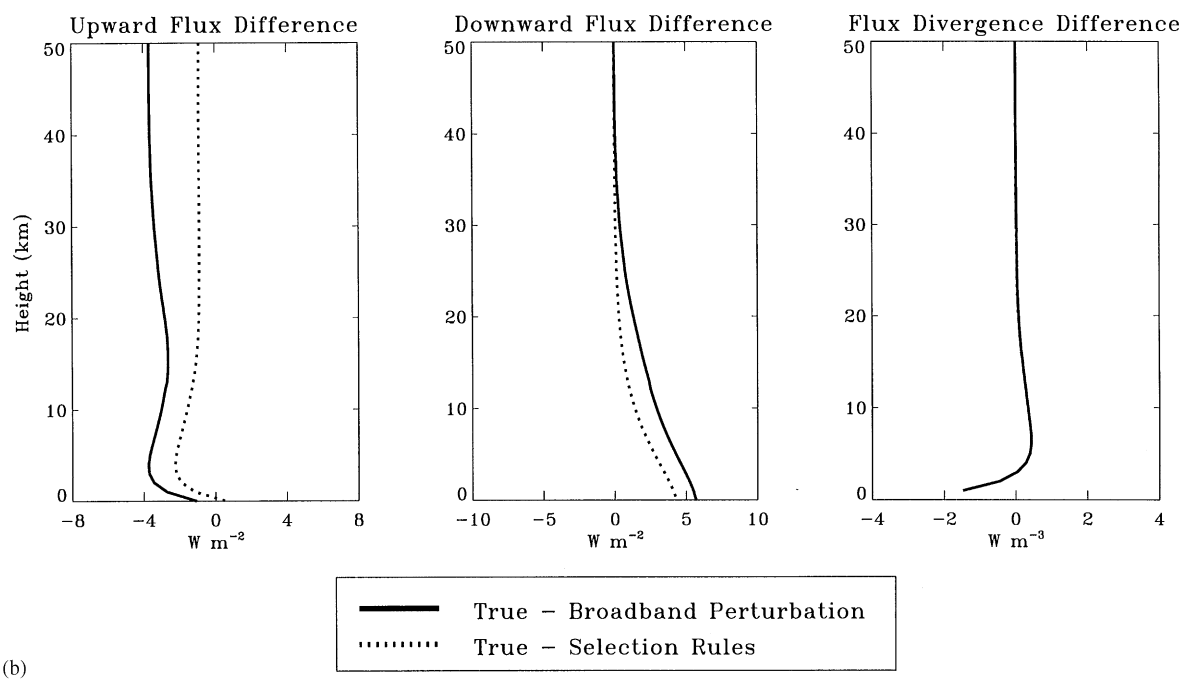

(b)

Fig. 10. (a) As in Fig. 8a with the exception that the underlying surface albedo was 0.2 and solar senith angle was 60° (b) Absolute errors in broadband fluxes computed from Fig. 10a.

solution of the physical fluxes for its determination. The practical consequence is that the adjoint is susceptible to numerical instabilities for optically thick, absorbing media. Numerical experiments suggest that the adjoint can be calculated accurately when multiple scattering prevails. (3) The physical flux and the adjoint flux are used to calculate perturbations. The technique derives from Eq. (1), and retains only first-order corrections to the base state. The latter consists of functions of the starting optical properties and is computed only once. Transitions to the final, desired state are accomplished via simple linear corrections. The aforementioned procedures lead to a semi-analytical solution. The numerical component enters twice through the calculation of coefficients required by the flux and adjoint. These coefficients are found by a tri-diagonal solver. The computational complexity of the adjoint is $2N_L^2$, where N_L designates the number of layers. The problem associated with numerical instability was in large measure overcome by developing selection rules. These rules can be used with either a standard two-stream solver or with adjoint perturbations. The method is useful in broadband calculations and is based on the idea that if absorption is dominant everywhere inside a medium, or if the medium is optically thin in all of its layers, then multiple scattering can be turned off and only the direct beam contribution need be calculated. The accuracy is determined by selecting an ω_T and σ_s. If a layer is strongly absorbing or weakly scattering, then a counter is incremented. This test is performed for all layers, and if the count is equal to the number of layers, only the direct beam is calculated. The perturbation-selection rules method has been applied successfully to atmospheres whose optical properties were specified according to the Fu and Liou's *k*-distribution model [9]. Based on the cases presented, we conclude that: (1) For the clear sky, the relative accuracy attainable in the broadband fluxes (using conventional adding) have been observed to be within 7% of the benchmark, while the computational gain was greater than an order of magnitude over the full up two-stream treatment. The sensitivity of the broadband fluxes to the selection of the base state was low. (2) For the cloudy sky, broadband fluxes show some sensitivity to the selection of the base state because the accuracy the adjoint fluxes can be calculated is related to the amount of absorption. However, use of selection rules with the conventional adding method yields gains spanning the range from 1.8 to nearly a 7-fold increase in speed. The adjoint-perturbation technique has also been demonstrated in a spectral application. In this application an entire atmospheric column, comprised of 19 layers was shown to yield accurate fluxes when both the scattering and extinction coefficients were everywhere perturbed by (the same) factors spanning the range 0.5–1.75. In this series of numerical experiments, multiple scattering was dominant. If the time taken for the computation of the base state is excluded, computational gains of 12 were observed per radiative transfer calculation. This computational gain assumes that fluxes are calculated at all layers, as they must if the conventional approach is used. However, if fluxes are required at fewer positions, the compuational gains increase. Unlike the standard adding method, the adjoint-perturbation method does not require that fluxes be calculated simultaneously everywhere. The problem of selecting an optimal base states for the cloudy atmosphere is the subject of ongoing research.

Acknowledgements

This research was supported by the Enviornmental Sciences Division of the Biological and Enviornmental Research (BER) Program under the U.S. Department of Energy Contract

DE-FG03-94ER61748 as part of the Atmospheric Radiation Measurement (ARM) Program. We wish to thank Dr. Renata McCoy for her thorough proofreading of this manuscript.

References

[1] Gabriel P, Harrington YJ, Stephens GL, Schneider TL. JQSRT 1998;59:1.
[2] Box MA, Gerstel SAW, Simmer C. Beitr Phys Atmosph 1988;61:301.
[3] Gerstel SAW. Applications of modern neutron transport methods to atmospheric radiative effects. International Radiation-Symposium. Fort Collins, Colorado, 11–16 August 1980. p. 500.
[4] Bell GI, Glasstone S. Nuclear reactor theory. New York, NY: Van Nostrand Reinholt, 1970.
[5] Loughlin PE, Box MA. Investigating biological response in the UV-B as a function of ozone variation using perturbation theory. Beitr Phys Atmosph, submitted.
[6] Box MA, Loughlin PE, Samaras M, Trautmann T. J Geophys Res 1997;102:4333.
[7] Box MA, Keevers M, McKellar BHJ. JQSRT 1987;39:219.
[8] Goody RM, Yung YL. Atmospheric radiation: theoretical basis. New York, NY: Oxford University Press, 1989.
[9] Fu Q, Liou K-N. J Atmos Sci 1992;49:2134.
[10] Wolfram S. Mathematica: a system for doing mathematics by computer. Redwood City: Addison-Wesley Publ. Comp. Inc., 1991.